© 2017. Published by The Company of Biologists Ltd | Development (2017) 144, 3777-3788 doi:10.1242/dev.149120

RESEARCH ARTICLE

The receptor protein tyrosine phosphatase PTPRB negatively regulates FGF2-dependent branching morphogenesis

Kelly J. Soady[1], Giusy Tornillo[2,‡], Howard Kendrick[2,‡], Valerie Meniel[2], Daria Olijnyk-Dallis[3,*], Joanna S. Morris[4], Torsten Stein[3], Barry A. Gusterson[3], Clare M. Isacke[1] and Matthew J. Smalley[2,§]

ABSTRACT

PTPRB is a transmembrane protein tyrosine phosphatase known to regulate blood vessel remodelling and angiogenesis. Here, we demonstrate that PTPRB negatively regulates branching morphogenesis in the mouse mammary epithelium. We show that *Ptprb* is highly expressed in adult mammary stem cells and also, although at lower levels, in oestrogen receptor-positive luminal cells. During mammary development, *Ptprb* expression is downregulated during puberty, a period of extensive ductal outgrowth and branching. *In vivo* shRNA knockdown of *Ptprb* in the cleared mammary fat pad transplant assay resulted in smaller epithelial outgrowths with an increased branching density and also increased branching in an *in vitro* organoid assay. Organoid branching was dependent on stimulation by FGF2, and *Ptprb* knockdown in mammary epithelial cells resulted in a higher level of fibroblast growth factor receptor (FGFR) activation and ERK1/2 phosphorylation, both at baseline and following FGF2 stimulation. Therefore, PTPRB regulates branching morphogenesis in the mammary epithelium by modulating the response of the FGFR signalling pathway to FGF stimulation. Considering the importance of branching morphogenesis in multiple taxa, our findings have general importance outside mammary developmental biology.

KEY WORDS: Mammary stem cells, Branching morphogenesis, PTPRB, FGFR2, Terminal end bud gene expression, Mouse

INTRODUCTION

The mammary gland is a highly dynamic organ; limited embryonic development is followed by extensive postnatal pubertal development with further differentiation and tissue remodelling occurring during pregnancy and lactation (Macias and Hinck, 2012). A key aspect of mammary epithelial structure formation is branching morphogenesis, a patterning event driven by systemic and local cues (Sternlicht, 2006). During pubertal development, branching morphogenesis is dependent on the balance between the rate of ductal extension driven by terminal end buds (TEBs; specialised growth structures at the tips of the developing ducts), the rate of TEB bifurcation and, in the later stages of development, the formation of lateral branches from established ducts. As branching morphogenesis is a common developmental process in many tissues in many taxa, understanding its regulation in the mammary gland could have implications beyond a single system and be applicable to similar aspects of development across the animal kingdom.

The growth of TEBs, and thus of the subtending ducts, is driven by one or more stem cell population(s) which generate the two main mammary epithelial lineages ('basal' and 'luminal') during puberty (Ball, 1998; Srinivasan et al., 2003; Williams and Daniel, 1983). Stem cells dispersed throughout the mature mammary epithelium are also thought to be important for maintenance of the adult non-pregnant gland, although the nature of these remains controversial (Rios et al., 2014; Van Keymeulen et al., 2011; Wang et al., 2015). It is clear, however, that the basal layer contains a small population of cells with potent outgrowth potential that, upon mammary fat pad transplantation, are able to regenerate complete basal and luminal layers, consistent with a stem cell identity (Shackleton et al., 2006; Sleeman et al., 2006; Stingl et al., 2006). In addition to this transplantable stem cell population, the basal layer consists mainly of contractile myoepithelial cells. The luminal layer consists of populations of progenitors (Regan et al., 2012) as well as functionally differentiated cells, including hormone-sensing oestrogen receptor (ER)-positive (ER^+) cells and the secretory ER negative (ER^-) cells found in the alveoli during lactation. The luminal progenitors are mainly ER^- (Regan et al., 2012). The molecular regulation of epithelial homeostasis in these stem-progenitor-differentiated populations, and how this homeostasis contributes to tissue morphogenesis, remains an area of intense interest.

PTPRB, also known as RPTPβ and VE-PTP, is a highly promiscuous R3 type receptor protein tyrosine phosphatase that can dephosphorylate multiple receptor tyrosine kinases (Barr et al., 2009). It consists of a single intracellular catalytic domain with C-terminal phosphorylation sites, a transmembrane domain and an extracellular domain with multiple fibronection type III-like domains (Matozaki et al., 2010). Binding by heparin binding domain-containing growth factors, such as pleiotropin, causes dimerisation and inactivation (Maeda and Noda, 1998). The role and functions of PTPRB have been most fully described in the development of the embryonic vasculature (Baumer et al., 2006; Dominguez et al., 2007) and in arterial endothelial cells, in which the two main targets of PTPRB have been identified as the receptor tyrosine phosphatase TEK and vascular endothelial cadherin (VE-cadherin; also known as cadherin 5 or CDH5). PTPRB activity enhances VE-cadherin-mediated adhesion (Nawroth et al., 2002) but is a negative regulator of TEK (Baumer et al., 2006; Dominguez et al., 2007).

[1]Division of Breast Cancer Research, Breast Cancer Now Research Centre, The Institute of Cancer Research, 237 Fulham Road, London SW3 6JB, UK. [2]European Cancer Stem Cell Research Institute and Cardiff School of Biosciences, Cardiff University, Hadyn Ellis Building, Maindy Road, Cardiff, CF24 4HQ, UK. [3]Institute of Cancer Sciences, College of Medical, Veterinary and Life Sciences, University of Glasgow, Glasgow, G12 8QQ, UK. [4]School of Veterinary Medicine, College of Medical, Veterinary and Life Sciences, University of Glasgow, Bearsden Road, Glasgow, G61 1QH, UK.
*Present address: Roslin Cell Therapies Ltd, NINE Edinburgh bioQuarter, 9 Little France Drive, EH16 4UX, Edinburgh, UK.
‡These authors contributed equally to this work

§Author for correspondence (SmalleyMJ@Cardiff.ac.uk)

K.J.S., 0000-0002-8274-7831; M.J.S., 0000-0001-9540-1146

Received 16 January 2017; Accepted 25 August 2017

Development (2017) 144, 3777-3788 doi:10.1242/dev.149120

We recently identified a set of 323 genes, including *Ptprb*, expression of which was specifically associated with the transplantable basal mammary stem cell (MaSC) population in the adult mouse mammary epithelium (Soady et al., 2015). As a regulator of morphogenesis in other systems, we hypothesised that PTPRB might also be a regulator of mammary development. However, owing to the embryonic lethality of *Ptprb* gene ablation and the lack of a conditional knockout model, the functional role of PTPRB in postnatal mammary gland development has not previously been studied. We have, therefore, exploited the potential of cleared fat pad transplantation in an *in vivo* functional genomics approach as well as *in vitro* mechanistic studies to determine whether PTPRB is required for normal mammary morphogenesis. We find that PTPRB is a negative regulator of branching morphogenesis, acting by modulating signalling downstream of FGFR. These results have general importance for understanding the regulation of epithelial branching morphogenesis.

RESULTS

Expression patterns of *Ptprb* in the mammary epithelium alter during postnatal mammary development

In an Affymetrix microarray-based analysis of gene expression in the adult (10- to 12-week-old) mammary epithelium comparing highly purified MaSCs with the other major epithelial subpopulations (myoepithelial cells, luminal ER^- progenitors and luminal ER^+ differentiated cells), we identified a 323 MaSC gene signature that included *Ptprb* (Soady et al., 2015). We hypothesised that PTPRB might be a regulator of mammary morphogenesis.

To test this hypothesis, we evaluated *Ptprb* expression by quantitative real-time reverse transcriptase PCR (qPCR) during postnatal mammary gland development in highly purified primary mammary epithelium subpopulations isolated by flow cytometry at three developmental time points. MaSC, myoepithelial (MYO), luminal ER^- progenitor ($LumER^-$) and luminal ER^+ differentiated ($LumER^+$) cells were isolated from female FVB/N mice as previously described (Regan et al., 2012; Soady et al., 2015) (Fig. S1). The developmental stages assessed covered pubertal mammary gland morphogenesis with three time points representing the onset/early stages of pubertal development (3-4 weeks), mid-puberty (5-6 weeks) and late puberty/young adulthood (8-10 weeks) (Fig. 1A).

Comparison of expression levels between the cell populations at each time point (Fig. 1B) demonstrated that at onset of puberty *Ptprb* was more highly expressed in $LumER^+$ cells than in MaSCs ($P \leq 0.01$). At mid-puberty, when the majority of ductal outgrowth occurs, *Ptprb* expression was not significantly different between the MaSCs and $LumER^+$ populations. Confirming our previous findings from the adult gland (Soady et al., 2015), at 8-10 weeks *Ptprb* was most highly expressed ($P \leq 0.01$) in MaSCs. However, at all time points, both MaSCs and $LumER^+$ cells had significantly higher levels of *Ptprb* expression than the $LumER^-$ and MYO populations.

Comparing expression levels between the time points within each cell subpopulation (Fig. 1C) showed that for each population *Ptprb* expression was reduced at 5-6 weeks (the period of most extensive epithelial expansion and morphogenesis) compared with expression levels at 3-4 weeks ($P \leq 0.05$ for $LumER^-$ cells, $P \leq 0.01$ for MYOs, MaSCs and $LumER^+$ cells). By 8-10 weeks, *Ptprb* expression in MaSCs had returned to 3-4 week levels; however, for the $LumER^+$ and MYOs, although *Ptprb* expression levels were increased compared with 5-6 week levels, they remained significantly lower than at 3-4 weeks old ($P \leq 0.01$ for both populations).

Consistent with the qPCR expression analysis, and the known role of PTPRB in endothelial cells, RNAScope *in situ* hybridisation localised *Ptprb* to the endothelial cells of blood vessels in the 3-week-old mammary gland and to a subset of luminal epithelial cells in mammary ducts (Fig. S2). In the 6-week-old gland, *Ptprb* expression could not be detected in the mammary epithelium, either because the numbers of cells expressing *Ptprb* was very low, or, the expression level per cell had fallen below the threshold for detection by the technique. However, at this time *Ptprb* was expressed in a group of stromal cells surrounding the ducts. Finally, at 12 weeks *Ptprb* was again detected in a subset of luminal cells although at much weaker levels (Fig. S2), consistent with the qPCR. We did not observe basal cells with a *Ptprb* signal at any age; however, basal mammary stem cells are very rare and indeed have never been definitively identified in histological sections, so this is not surprising.

As *Ptprb* expression was below the limits of detection by *in situ* hybridisation at 6 weeks, to determine whether *Ptprb* was differentially expressed in the two main morphological structures of the developing gland, the TEBs and their subtending ducts, a gene expression profile data set of microdissected TEBs compared with ducts collected at 6-7 weeks was mined for *Ptprb* expression (Table S1). This analysis demonstrated that *Prprb* is expressed at significantly lower levels in the TEBs compared with the ducts (1.5-fold lower; $P<0.05$).

In summary, *Ptprb* is most highly expressed in MaSCs and $LumER^+$ cells in the adult mammary epithelium, but its expression pattern is dynamically regulated during pubertal development. $LumER^+$ cells have a decrease in *Ptprb* expression at mid-puberty followed by a partial recovery; MaSCs also have a decrease in mid-puberty but a strong recovery in the adult tissue back to levels seen at pubertal onset. During puberty, *Ptprb* is expressed at lower levels in TEBs than in ducts. The strong recovery of expression in MaSCs compared with the partial recovery in $LumER^+$ cells results in the MaSCs becoming the highest expressers of *Ptprb* in the adult gland.

Ptprb knockdown promotes branching morphogenesis *in vivo*

The correlation between lower levels of *Ptprb* expression and the period of most intense morphogenetic activity in the mammary gland, suggested that PTPRB may be a negative regulator of mammary morphogenesis. We tested this in *in vivo* functional assays. In the first series of experiments, primary mouse mammary epithelial cells were transduced in short-term culture (48 h) with either a pooled lentiviral supernatant containing two shRNA sequences against *Ptprb* (shPtprb pool consisting of shPtprb 0145 plus shPtprb 3820) or a control shRNA designed to target luciferase (shLuc). In a second series of three independent experiments, primary cells were transduced in short-term culture with one of two different lentiviral constructs carrying shRNA sequences targeting *Ptprb* (shPtprb 0145 or shPtprb 3820) or with a lentvirus carrying a scrambled sequence (shScr). In both sets of experiments the viral vectors also contained GFP to mark transduced cells and supernatants were diluted to ensure both control and shPtprb supernatants contained equal viral titres. The efficacy of the shPtprb pool and the individual lentiviruses in suppressing *Ptprb* expression was confirmed by qPCR (Fig. 2A,B). Transduced cells were transplanted into cleared mammary fat pads at 50,000 cells per fat pad. At 8 weeks, fat pads were harvested and examined under epifluorescent illumination, after which they were processed for flow cytometric analysis to assess the relative proportions of the epithelial cell populations.

Development (2017) 144, 3777-3788 doi:10.1242/dev.149120

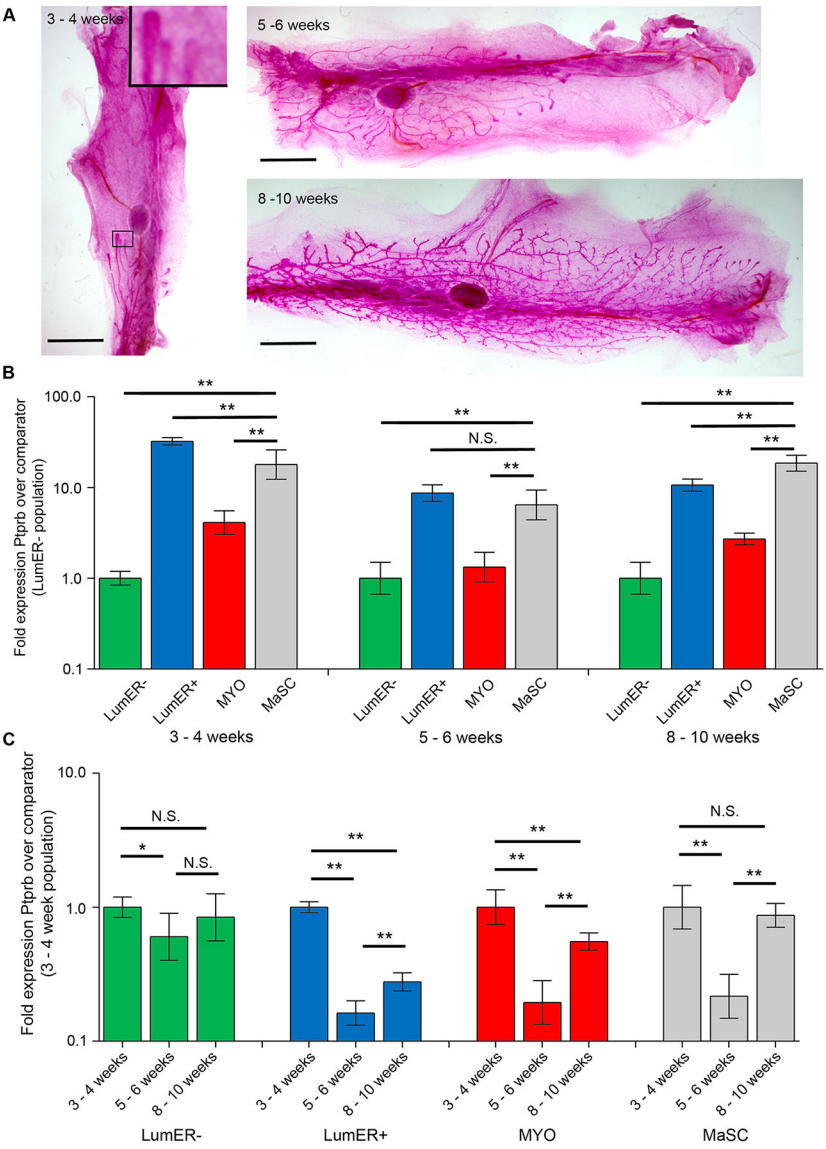

Fig. 1. Ptprb expression is repressed in mid-pubertal mammary epithelial cells. (A) Whole-mount fourth mammary fat pads from FVB/N mice at 3-4, 5-6 and 8-10 weeks of age illustrating the extent of ductal development. Scale bars: 3 mm. Inset shows enlargement (5×) of the boxed area of the 3-4 week fat pad to show terminal end buds. (B) Relative *Ptprb* expression between MaSC and MYO, MaSC and LumER^{-}, and MaSC and LumER^{+} populations determined by qPCR at three time points. The comparator sample is the LumER^{-} population at each age group. (C) Relative *Ptprb* expression within each population across the three time points. Comparator was the 4-week-old sample for each population. Significance comparisons between 3-4 week and 5-6 week, between 3-4 week and 8-10 week and between 5-6 week and 8-10 week populations are indicated. $^{**}P<0.01$, $^{*}P<0.05$, N.S., not significant. Data in B and C were from three independent isolates of each cell population at each age. Data were normalised to β-actin (*Actb*) and expressed as mean log10 relative fold expression (±95% confidence intervals) over the comparator.

There were no differences in the number of successful outgrowths between the shLuc (8 outgrowths from 11 transplanted fat pads; n=2 independent experiments) and the shPtprb pool (11/11; n=2 independent experiments) transplants or between the shScr (23/24; n=3 independent experiments), the shPtprb 0145 (13/13; n=3 independent experiments) and the shPtprb 3820 (11/13; n=3 independent experiments) transplants. However, *Ptprb*-knockdown transplants appeared to be more densely branched but filled less of the total area of the fat pad than the control outgrowths (Fig. 2C). Quantification of the area of the outgrowths and of the number of branch points per mm^2 confirmed that knockdown outgrowths were significantly smaller than control outgrowths, but were more densely branched (Fig. 2D,E).

Both control and *Ptprb*-knockdown outgrowths had distinct luminal [keratin 18 (K18; KRT18) positive] and basal/myoepithelial [smooth muscle actin (SMA; ACTA2) positive] layers (Fig. 3A). Flow cytometric analysis of the outgrowths confirmed that there were no differences in the proportions of the major epithelial populations (Fig. S3). Ki67 (Mki67) staining of control and *Ptprb*-knockdown transplants demonstrated that, at the time point at which the transplants were harvested, there was little or no proliferation in control tissue but *Ptprb*-knockdown tissue was highly proliferative (Fig. 3B). However, the smaller size and denser branching of the knockdown tissue (meaning that sections were more likely to be enriched for the TEBs) is an important caveat in this analysis. In the proliferating *Ptprb*-knockdown tissue, equivalent numbers of Ki67-positive cells were observed in SMA-positive basal and SMA-negative luminal layers (Fig. 3B,C). Little or no cleaved caspase-3, a marker of apoptosis, could be detected in either control or *Ptprb*-knockdown outgrowths (Fig. S4B).

To determine whether *Ptprb* knockdown perturbed stem cell function, as assessed by engraftment potential, GFP-positive regions from a series of successful shScr and shPtprb 0145 primary transplants were dissected out, digested to single cells and then re-transplanted. Take rates for secondary transplantation into contralateral fat pads of shScr- and shPtprb 0145-transduced cells were 8/9 for both the control and knockdown cells. Consistent with the primary transplants, shPtprb 0145-transduced outgrowths had a significantly smaller area than control outgrowths (Fig. 3D, Fig. S4C). Overall, these findings show PTPRB does not affect stem cell engraftment potential or lineage determination, but does regulate mammary branching morphogenesis.

Development (2017) 144, 3777-3788 doi:10.1242/dev.149120

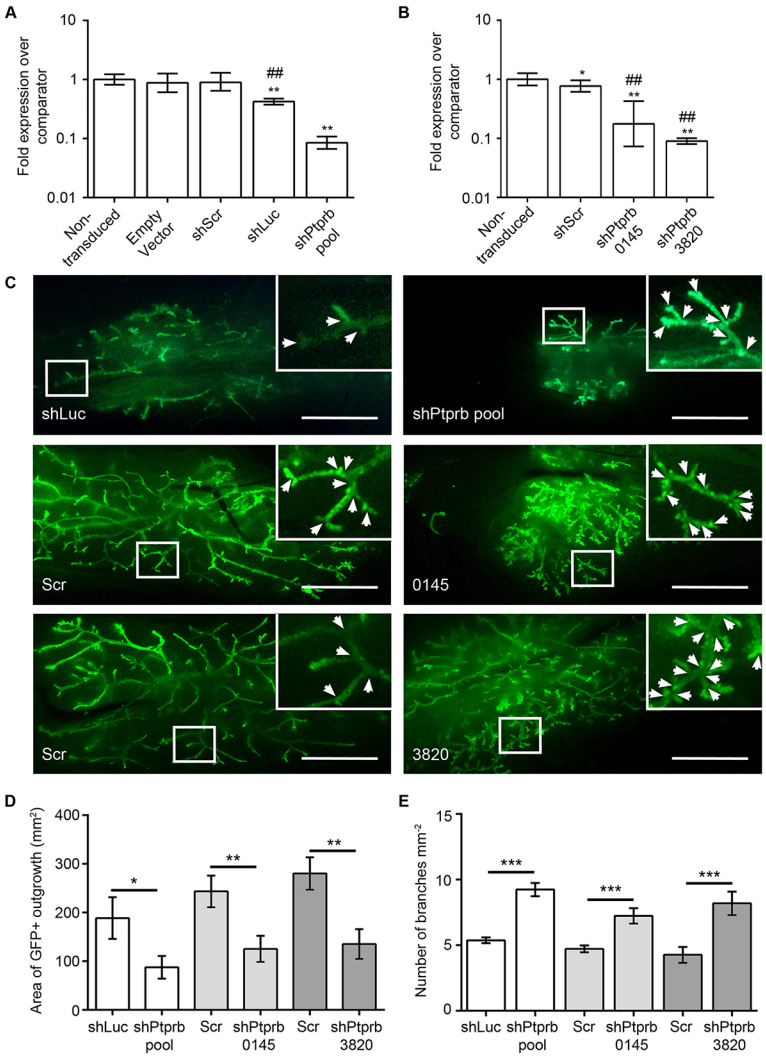

Fig. 2. *Ptprb* knockdown promotes branching morphogenesis *in vivo*. (A) qPCR analysis of *Ptprb* gene expression in non-transduced primary mouse mammary epithelial cells and in cells transduced with either an empty virus, a control virus carrying a scrambled oligonucleotide sequence (shScr), a sequence targeting luciferase (shLuc), or a virus pool consisting of two viruses (shPtprb 0145 and 3820) targeting *Ptprb*. (B) qPCR analysis of *Ptprb* gene expression in non-transduced cells and cells transduced with shScr virus or the individual shPtprb 0145 and shPtprb 3820 viruses. Data in A,B are presented as mean fold *Ptprb* expression (±95% confidence intervals; n=3 independent experiments) over comparator (non-transduced cells). *P<0.05 compared with non-transduced cells; **P<0.01 compared with non-transduced cells; ##P<0.01 compared with shLuc or shScr-transduced cells. (C) Representative images of GFP$^+$ outgrowths in whole-mount fat pads 8 weeks after transplant of control- or shPtprb-transduced cells. Scale bars: 5 mm. Insets show enlargements (×3) of the boxed areas. Branch points in insets are indicated by arrowheads. For each shPtprb fat pad, the control shown next to it is a transplanted contralateral gland from the same animal. (D,E) Analysis of size (D) and branching (E) of control and shPtprb knockdown outgrowths (mean±s.e.m.). *P<0.05, **P<0.01, ***P<0.001. shLuc and shPtprb data from two independent transplant experiments; shScr, shPtprb 0145 and shPtprb 3820 data from three independent experiments. Numbers of fat pads analysed are provided in Fig. S4A.

Ptprb knockdown promotes branching morphogenesis in an *in vitro* model system in an FGF-dependent manner

To provide further support for a role for PTPRB in regulating branching morphogenesis and to establish a model in which the mechanism of action of PTPRB could be addressed, we utilised an *in vitro* branching morphogenesis assay (Ewald et al., 2008). Small fragments of mammary epithelial ducts, which retain the basal-luminal bilayered architecture (‘organoids’), were either left untransduced or transduced with shScr, shPtprb 0145 or shPtprb 3820 lentiviruses, embedded in Matrigel and treated for 5 days with medium containing FGF2, which stimulates branching in this system (Ewald et al., 2008). The total number of organoids and number of branched organoids were counted; branched organoids were defined as an organoid with at least one branch protruding from the main spherical body.

Organoid cultures branched only in the presence of FGF2; in the absence of FGF2, *Ptprb* knockdown alone was not sufficient to stimulate branching (Fig. S5A). However, knockdown of *Ptprb* in FGF2-stimulated cultures significantly increased (P≤0.05) the number of branched organoids, with 40% of organoids branching in non-infected and Scr controls compared with >60% in shPtprb1 0145 and shPtprb2 3820 cultures (Fig. 4A). The amount of branching in non-infected and Scr controls was consistent with previous reports on branching in unmanipulated primary mammary epithelial organoids (Macias et al., 2011). Therefore, *Ptprb* knockdown *in vitro* increased the number of organoids competent to branch under FGF2 stimulation.

To assess whether *Ptprb* knockdown also affected the extent of branching, the degree of branching in all branched organoids was ascertained. Branched organoids were categorised into low (1-5 branches), intermediate (6-15 branches) or highly branched (>15 branches) organoids (Fig. 4B,C). Compared with control cultures, shPtprb 0145- and shPtprb 3820-transduced organoids had an increase in the proportion of highly branched organoids and a reduction in numbers of organoids with low branching levels (Fig. 4C). Therefore, *in vitro* knockdown of *Ptprb* increased both the percentage of branched mammary epithelial organoids and the number of branches on each branched organoid, but only under conditions of growth factor stimulation.

Endogenous *Ptprb* expression is downregulated during *in vitro* branching morphogenesis

In vivo, levels of endogenous *Ptprb* expression are suppressed during the period of postnatal mammary development. To determine if similar changes in *Ptprb* expression occur during organoid branching *in vitro*, and to characterise in more detail the relationship between the kinetics of endogenous *Ptprb* expression

Development (2017) 144, 3777-3788 doi:10.1242/dev.149120

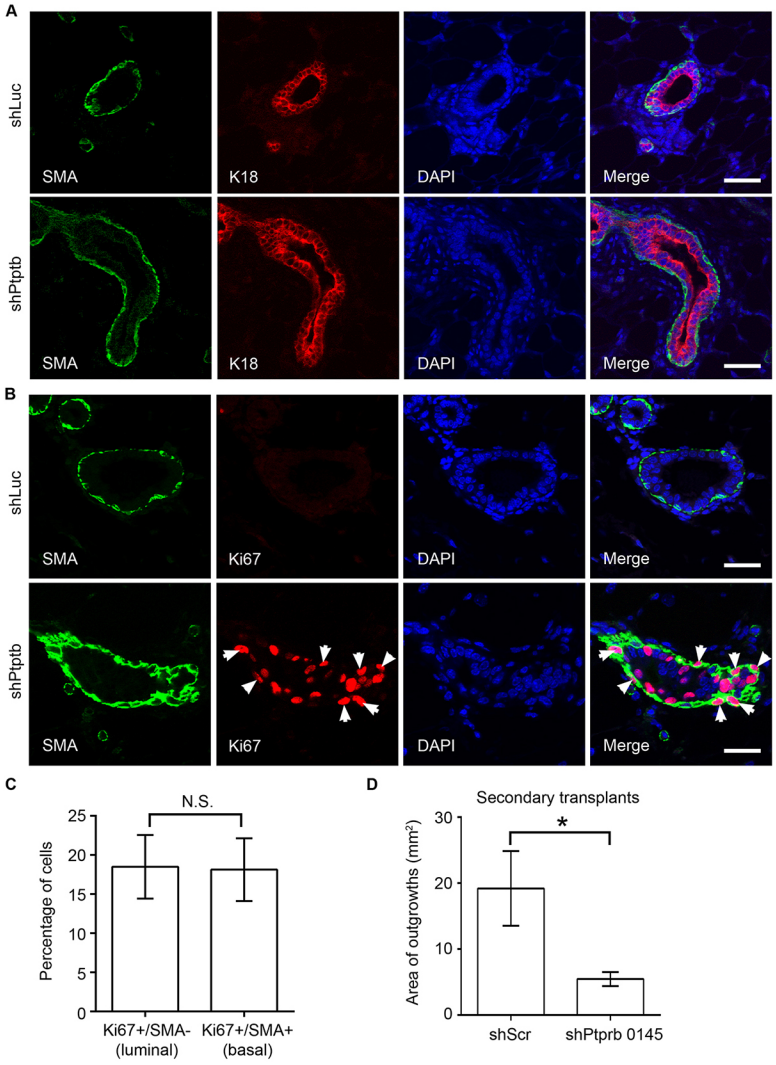

Fig. 3. *Ptprb* knockdown increases mammary epithelial cell proliferation. (A,B) Staining of sections of shLuc (top rows) and shPtprb (bottom rows) outgrowths with anti-SMA and DAPI and either anti-K18 (A) or anti-Ki67 (B) antibodies. Arrowheads indicate Ki67-positive basal (SMA^+) cells. Scale bars: 100 µm. (C) Quantification of Ki67 staining in luminal (SMA^-) and basal (SMA^+) layers of shPtprb outgrowths. Data are shown as mean±s.e.m. (n=8 regions from three independent control outgrowths and 11 regions from three independent Ptprb-knockdown outgrowths). (D) Analysis of areas (mm^2) of outgrowths of shScr (n=8) and shPtprb 0145 (n=8) secondary transplants (mean±s.e.m.). *P<0.05; N.S., not significant.

and branching, unmanipulated non-infected organoids were embedded in Matrigel and stimulated with or cultured without FGF2 for 6 days. Non-stimulated organoids did not grow or branch over the experimental time course whereas stimulated organoids expanded in size and produced branches, with the first obvious branching apparent by day 4 (Fig. 5A). qPCR analysis of *Ptprb* expression in FGF2-stimulated branching organoids showed that *Ptprb* expression was reduced over time in stimulated organoids relative to day 0. The reduction in *Ptprb* expression was significant from day 1, decreased further at day 3 and remained low until the end of the time course (Fig. 5B).

To control for the possibility that the decrease in *Ptprb* expression was related to the time in culture rather than correlated with FGF2 stimulation and concomitant branching, levels of *Ptprb* expression in stimulated organoids were compared with non-stimulated organoids at each time point (Fig. 5C). This demonstrated that *Ptprb* expression in stimulated organoids was significantly lower than in non-stimulated organoids by day 3 and continued to drop at days 4 and 5. Importantly, these findings showed that the first significant difference between *Ptprb* levels in non-stimulated and stimulated organoids was seen just before (day 3) the stimulated organoids initiated branching (day 4). This suggests a temporal correlation between FGF2 stimulation, *Ptprb* expression and branching.

PTPRB acts on FGFR-ERK1/2 signalling to inhibit mammary branching morphogenesis

The *in vivo* and *in vitro* findings, taken together, suggested that although PTPRB does not directly inhibit mammary morphogenesis, it acts as a negative regulator of signalling pathways that promote branching morphogenesis. In this model, suppression of *Ptprb* expression would result in either a higher or more sustained level of signalling by pro-branching pathways. Using an organoid culture system, we have already demonstrated that *Ptprb* expression interacted with FGF signalling *in vitro*. To determine whether there was evidence for an interaction between PTPRB and FGF signalling *in vivo*, and to assess the possibility that PTPRB regulates other signalling pathways associated with mammary branching morphogenesis, we used qPCR to examine the expression of three receptor tyrosine kinases (*Erbb2*, *Egfr* and *Tek*) previously suggested to interact with PTPRB and with potential roles in mammary branching morphogenesis (Andrechek et al., 2005; Chodosh et al., 2000; Wiesen et al., 1999). We also examined expression of three receptor kinases, including two members of the FGF receptor family (*Fgfr1*, *Fgfr2* and *Igf1r*), not previously described as interacting with PTPRB but known to play an important role in mammary development (Lu et al., 2008; Pond et al., 2013; Sternlicht et al., 2006). Patterns of expression in the different mammary epithelial subpopulations at the 5-6 week

Development (2017) 144, 3777-3788 doi:10.1242/dev.149120

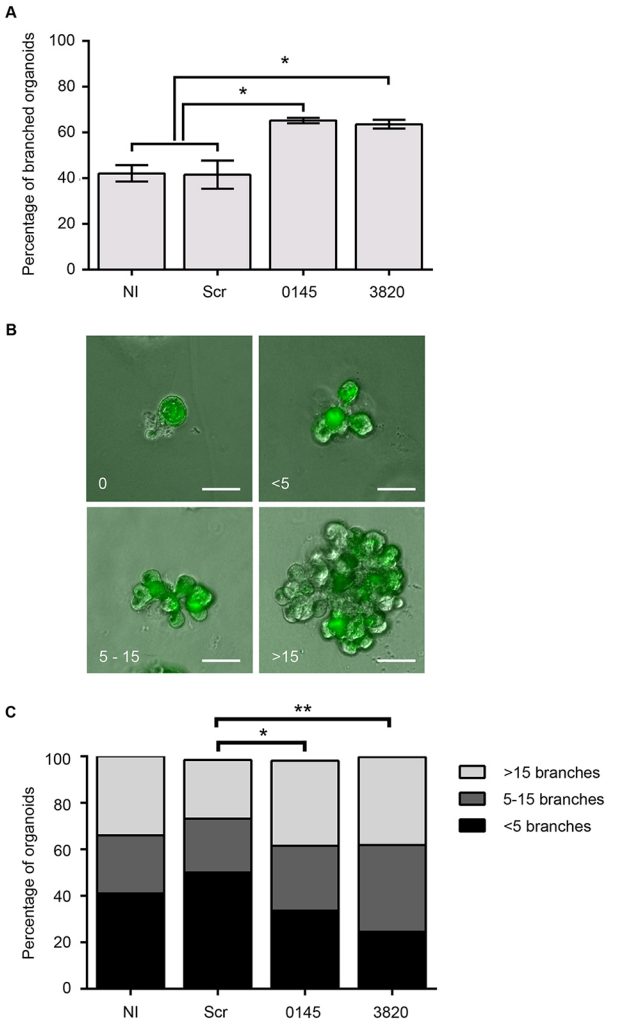

Fig. 4. *Ptprb* knockdown promotes branching morphogenesis in an *in vitro* model system. Non-infected (NI), shScr-, shPtprb 0145- and shPtprb 3820-transduced organoids were embedded in Matrigel and stimulated to branch with FGF2 for 5 days in culture. Data from three independent experiments (duplicate wells for each treatment per experiment). GFP expression was used as a marker of lentivirus infection. (A) Number of branched organoids as a percentage of the total number of organoids (mean± s.d.). **P*<0.05 (*t*-test). (B) Representative images (merged GFP fluorescence and phase contrast) of organoids with no branching (0 branches), low-level branching (1-5 branches), intermediate-level branching (6-15) and high-level branching (>15). Scale bars: 30 µm. (C) Extent of branching in non-infected (NI), shScr and *Ptprb* knockdown organoids. The proportion of organoids with low-, intermediate- or high-level branching is shown as a percentage of the total number of branched organoids per treatment. **P*<0.05; ***P*<0.01 (χ^2 test of distribution of categorical variables).

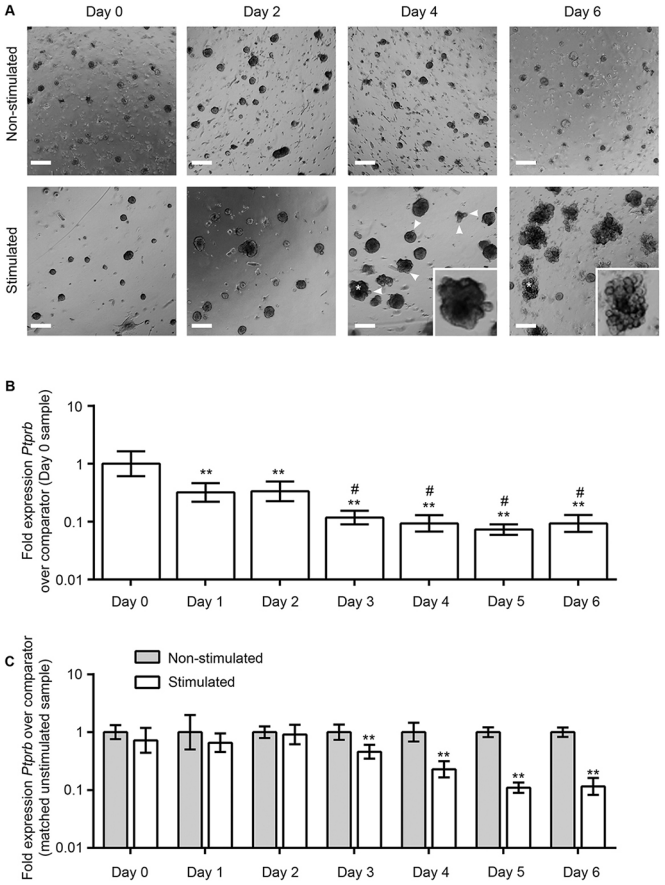

Fig. 5. FGF2 suppresses *Ptprb* expression *in vitro*. (A) Representative images of unmanipulated organoids in 3D culture either 'non-stimulated' (without growth factor; top panel) or 'stimulated' (with FGF2; bottom panel). Scale bars: 100 µm. Arrowheads indicate branches emerging at day 4. Insets show enlarged (2.5×) images of the organoids marked by asterisks. (B,C) *Ptprb* expression in non-stimulated and stimulated organoids, taken at 24 h time points for 6 days, determined by qPCR. Data normalised to β-actin (*Actb*) and expressed as mean log10 relative fold expression (±95% confidence intervals) over comparator population. Data were collected from three independent organoid preparations. (B) *Ptprb* expression in stimulated organoids using the day 0 time point as the comparator sample. ***P*<0.01 compared with day 0; $^{\#}P$<0.01 compared with day 2 (*t*-tests). (C) *Ptprb* expression in non-stimulated and stimulated organoids with expression levels in stimulated organoids compared with non-stimulated organoids at the same time point. ***P*<0.01 relative to comparator.

developmental time point (when branching morphogenesis in the mammary epithelium is maximal) were determined and compared with the previously established pattern of *Ptprb* expression (Fig. 6A). This analysis showed a strong correlation between *Ptprb* expression and the patterns of *Fgfr2* and *Tek* expression across the subpopulations, but no correlation with *Egfr*, *Fgfr1* or *Igf1r* expression.

Next, expression of *Fgfr2* and *Tek* across the 3-4 week, 5-6 week and 8-10 week time course was examined and compared with *Ptprb* (Fig. 6B,C). We concentrated on expression patterns in the MaSCs and LumER$^+$ cells, as these two populations showed the highest levels of *Ptprb*, *Fgfr2* and *Tek* at 5-6 weeks. Expression of *Tek* in LumER$^+$ cells was significantly lowered in 5-6 week animals relative to 3-4 weeks. However, by 8-10 weeks it was back to 3-4 week levels (Fig. 6B). By contrast, *Tek* levels in MaSCs were not significantly different between 3-4 weeks and 5-6 weeks and then fell significantly at 8-10 weeks. Thus, there were similarities between *Tek* and *Ptprb* expression patterns in LumER$^+$ cells, although these were not exact. However, there were no obvious correlations between *Tek* and *Ptprb* expression in MaSCs (Fig. 6C).

Fgfr2 expression levels were not significantly different in the LumER$^+$ cells between 3-4 weeks and 5-6 weeks but were significantly increased at 8-10 weeks. However, in MaSCs, there was a significant increase in *Fgfr2* expression at 5-6 weeks compared with 3-4 weeks. Therefore, there was no obvious correlation between *Ptprb* and *Fgfr2* expression in LumER$^+$ cells but there was an inverse correlation between the *Ptprb* and *Fgfr2* expression patterns in the MaSCs (Fig. 6B,C).

Development (2017) 144, 3777-3788 doi:10.1242/dev.149120

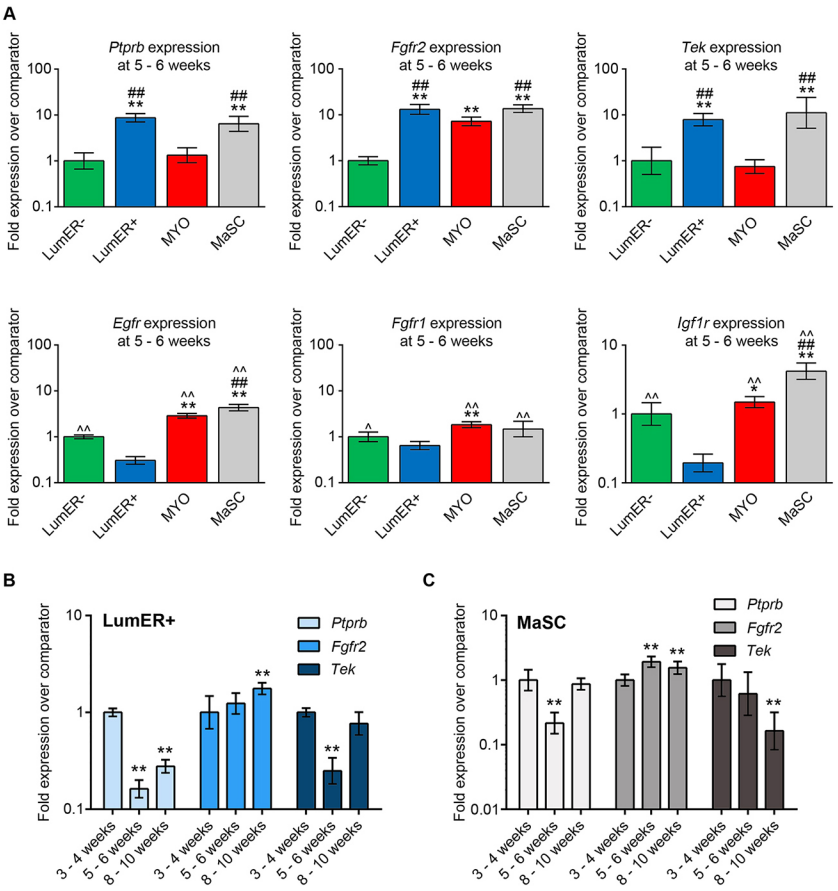

Fig. 6. Analysis of expression of candidate PTPRB-interacting receptor tyrosine kinases in mammary epithelial subpopulations. (A) Relative *Ptprb*, *Fgfr2*, *Tek*, *Egfr*, *Fgfr1* and *Igf1r* expression in MaSCs, MYOs, LumER^{-} and LumER^{+} populations determined by qPCR at mid-puberty (5-6 week samples). The comparator sample is the LumER^{-} population in all cases. *Ptprb* data reproduced from Fig. 1 for reference. $^{**}P$<0.01 versus LumER^{-}, $^{*}P$<0.05 versus LumER^{-}; $^{\#\#}P$<0.01 versus MYO, $\wedge\wedge P$<0.01 versus LumER^{+}, $\wedge P$<0.05 versus LumER^{+}. For simplicity, significance is only shown compared with lower expressing samples. (B,C) Relative *Ptprb*, *Fgfr2* and *Tek* expression in LumER^{+} cells (B) and MaSCs (C) at 3-4, 5-6 and 8-10 weeks of age. The comparator was the 4-week-old sample for each population. Data were normalised to β-actin (*Actb*) and expressed as mean log10 relative fold expression (±95% confidence intervals) over the comparator. Data from three independent isolates of each cell population at each age. *Ptprb* data reproduced from Fig. 1 for reference. $^{**}P$<0.01 versus 3-4 week samples.

The *in vitro* organoid assay had already demonstrated that treatment with the FGFR ligand FGF2 promotes branching morphogenesis whilst suppressing *Ptprb* expression, supporting the inverse correlative relationship between *Fgfr2* and *Ptprb* expression *in vivo*. We now tested whether two ligands for TEK, angiopoietin 1 and 2 (ANG1 and 2; also known as ANGPT1 and 2), could substitute for FGF2 in this assay. However, neither was able to stimulate branching (Fig. S5B), suggesting that the ANG-TEK axis is not involved in mammary branching morphogenesis. We therefore focussed on FGFR signalling and addressed whether PTPRB is a negative regulator of this pathway.

As PTPRB is a cell surface receptor phosphatase, we hypothesised that it might be regulating phosphorylation of FGF receptors. We therefore tested in three independent experiments whether *Ptprb* knockdown altered baseline levels of FGFR phosphorylation as well as the response to FGF2. Indeed, transduction with the shPtprb 3820 virus significantly increased FGFR phosphorylation over shLuc control, both baseline levels and in response to FGF2. The effects of shPtprb 0145 were more modest, with a significant difference only seen after five minutes of FGF2 treatment (Fig. 7A, Fig. S6). Note that pFGFR antibodies cannot distinguish between the FGFR receptor isoforms, so it is not possible to determine which (or indeed if more than one) of the family shows increased phosphorylation in response to *Ptprb* knockdown. However, by using non-phospho-specific antibodies which do distinguish between the isoforms, we were able to demonstrate that total levels of FGFR1, 2, 3 and 4 were not changed when *Ptprb* was knocked down (Figs S7 and S8), confirming that the increase in pFGFR levels was indeed due to increased receptor phosphorylation rather than to increased receptor expression.

We next tested whether *Ptprb* knockdown altered the response of a downstream effector of FGF signalling, ERK1/2 (also known as MAPK3/1), to FGF2. First, we confirmed that branching in the organoid culture system in response to FGF2 was dependent on ERK1/2 activity, using a small molecule inhibitor of ERK (SCH772984; Figs S9 and S10). Next, organoids cultured in the *in vitro* branching assay system were transduced with either shLuc, shPtprb 0145 or shPtprb 3820 knockdown virus and protein lysates collected either from unstimulated cultures or from cultures after 5, 15 and 60 min of FGF2 stimulation. In three independent experiments, *Ptprb* knockdown by both shPtprb 0145 and shPtprb 3820 resulted in a statistically significant increase in unstimulated baseline ERK1/2 phosphorylation compared with shLuc controls. In response to FGF2 stimulation, shPtprb 3820 cultures continued to show statistically significantly higher levels of phosphorylation at all time points, over and above the increased phosphorylation resulting from activation of the pathway. shPtprb 0145 cultures also showed higher mean phosphorylation but the differences in stimulated cultures were not statistically significant (Fig. 7B, Fig. S11).

Finally, FGF-stimulated organoids in which *Ptprb* had been knocked down by either shPtprb 0145 or shPtprb 3820, were treated with SCH772984. In control cultures, knockdown organoids showed increased branching in response to FGF, as previously. However, treatment with the inhibitor partially restored branching back to control levels in shPtprb 0145-transduced cultures and fully restored control branching levels in shPtprb 3820 cultures (Fig. 7C). Taken together, these findings support the model that PTPRB suppresses branching morphogenesis via inhibition of the FGFR2-ERK1/2 signalling axis.

Development (2017) 144, 3777-3788 doi:10.1242/dev.149120

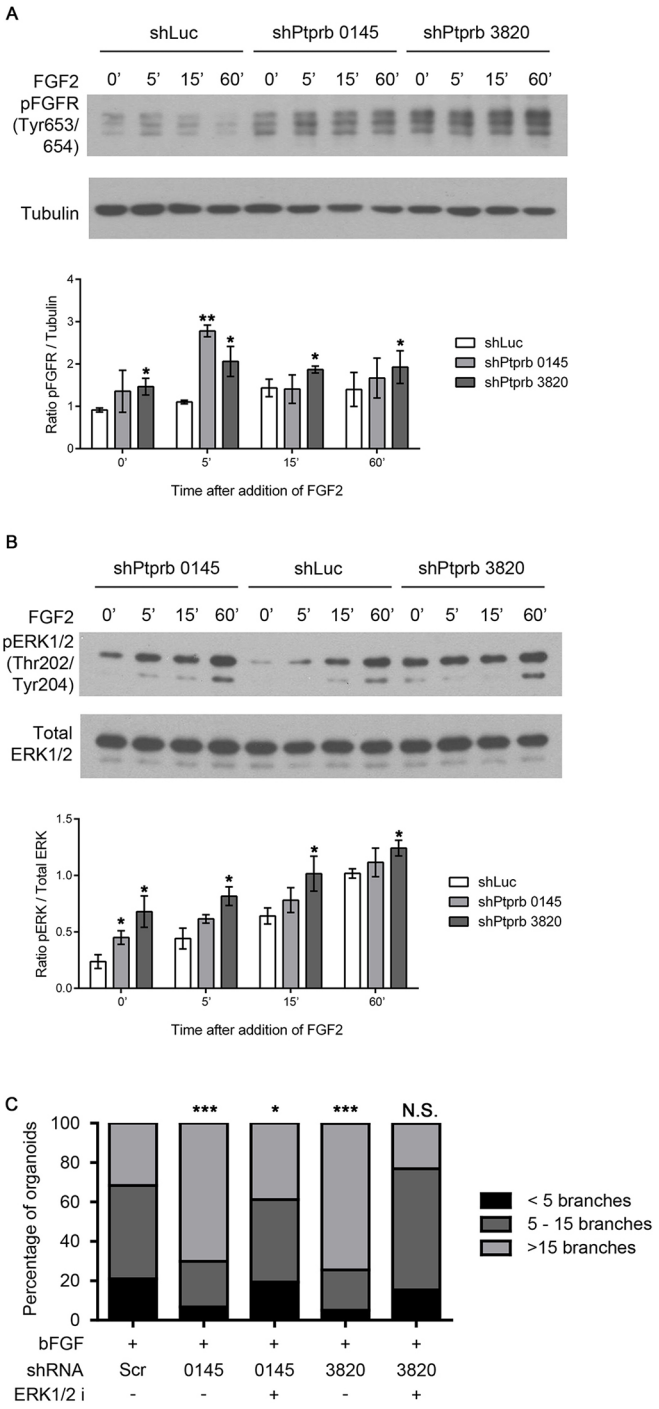

Fig. 7. PTPRB suppresses FGFR2 signalling by negatively regulating ERK1/2. (A,B) Western blot analysis of phospho-FGFR levels (A) and phospho- and total-ERK1/2 levels (B) in shLuc-, shPtprb 0145- and shPtprb 3820-transduced primary mouse organoid cultures either unstimulated or stimulated with FGF2 for 5, 15 and 60 min. Blots are representative of three independent experiments; quantification of phospho:total ERK1/2 ratios and phospho-FGFR:tubulin loading control ratios are shown next to the blots (mean±s.e.m.). *P<0.05 compared with shLuc control at that time point. The original blots are shown in Figs S6 and S11. (C) Extent of branching in bFGF-stimulated shScr-organoids (Scr) and *Ptprb* knocked-down organoids (0145 and 3820) stimulated with bFGF and treated (or not) with SCH772984 (2 nM; ERK1/2 i). *P<0.05; ***P<0.01 versus control FGF-stimulated samples (χ^2 test of distribution of categorical variables); N.S. not significant.

DISCUSSION

Mammary epithelial development is a highly regulated process dependent on the interplay between systemically acting hormones and locally produced growth factors. During puberty, rising levels of the ovarian steroid hormones oestrogen and progesterone, growth hormone secreted from the pituitary gland and locally produced growth factors cause a significant increase in ductal growth (Hennighausen and Robinson, 2001; Macias and Hinck, 2012). This growth is driven by bulbous TEBs, which form at the tips of elongating primary ducts and regularly bifurcate to form the primary branches of the ductal epithelium. As the mammary tree matures, secondary side branches sprout laterally at regular intervals, from which will form the tertiary lateral branches that occur at each dioestrus and during pregnancy. The TEB-tipped ducts grow until they reach the edge of the fat pad. At this stage, the TEBs regress and the subtending duct becomes relatively quiescent, leaving the branched ductal structures of the mature virgin gland (Hens and Wysolmerski, 2005). The unique 'open architecture' of the non-pregnant gland suggests that branching morphogenesis is a highly regulated process, involving orchestrated ductal elongation, TEB bifurcation and lateral branching, which ensures space for additional proliferation and the formation of alveoli during pregnancy. A number of positive regulators of this process have been reported, such as the oestrogen/oestrogen receptor alpha (ER) axis and its downstream effectors, the growth hormone/growth hormone receptor/insulin-like growth factor 1 axis, epidermal growth factor receptor (EGFR) signalling and FGFR signalling. However, few negative regulators have been identified, transforming growth factor beta 1 (TGFβ1) and sprouty 2 (SPRY2) being notable exceptions (Sternlicht, 2006; Sternlicht et al., 2006). Here, we have now identified PTPRB as a novel negative regulator of this process.

In arterial endothelial cells, PTPRB activity enhances VE-cadherin-mediated adhesion (Nawroth et al., 2002) but is a negative regulator of TEK. Use of PTPRB-inactivating antibodies in adult mice triggered activation of TEK, resulting in increased downstream signalling via ERK1/2, which in turn caused increased endothelial cell proliferation and enlargement of vascular structures (Winderlich et al., 2009). Thus, PTPRB is required to balance TEK activity and endothelial cell proliferation, thereby controlling blood vessel development and vessel size. This is supported by work in two independent germline *Ptprb* mouse knockout models, in which embryonic lethality occurred at around 10 days gestation owing to severe vascular defects. In both models, vasculogenesis occurred normally but angiogenesis was severely affected leading to the deterioration of the intra-embryonic vascular system and lethality, demonstrating an essential role for PTPRB in angiogenesis and blood vessel remodelling (Baumer et al., 2006; Dominguez et al., 2007).

In contrast to angiogenesis, in the mammary epithelium we find that PTPRB regulates morphogenesis by modulating FGFR signalling rather than TEK signalling. FGFRs can activate a number of potential downstream pathways, including PI3K/PIP2/AKT, PLCγ/IP3/Ca^{2+}/calmodulin and SOS/RAS/RAF/MEK/ERK. FGFR stimulates the SOS/RAS/RAF/MEK/ERK pathway by phosphorylation of fibroblast growth factor receptor substrate 2 (FRS2), which in turn recruits GRB2, activating SOS and the downstream cascade (Katoh, 2009). Notably, SPRY2, another negative regulator of branching morphogenesis (Sternlicht, 2006; Sternlicht et al., 2006) is a negative regulator of FGF-induced ERK pathway activation (Rubin et al., 2005), probably acting downstream of the GRB2-SOS complex (Gross et al., 2001).

Development (2017) 144, 3777-3788 doi:10.1242/dev.149120

Here, we have demonstrated that knockdown of PTPRB results in higher baseline levels of FGFR phosphorylation, resulting in higher levels of downstream p-ERK1/2 and a more sustained response to FGF2 stimulation, leading to a more densely branched mammary tree.

Evidence is emerging that *PTPRB* might be a tumour suppressor gene in a variety of cancers. Recurrent PTPRB loss-of-function mutations have been identified in angiosarcoma (in 10 of 39 tumours examined) (Behjati et al., 2014), consistent with its normal role in angiogenesis, but also in metastatic melanoma (9 tumours with missense, nonsense or splice-site mutations out of a 97 tumour set) (Ding et al., 2014). Homozygous single nucleotide variations in *PTPRB* have also been reported in a rare family with siblings with glioblastoma multiforme; the parents were heterozygous for the mutations (Backes et al., 2014). No specific study of PTPRB in breast cancer has been undertaken, although *Ptprb* is a component of the MaSC gene signature we have identified as being prognostic in breast tumours (Soady et al., 2015). In contrast, a link between FGFR2 and breast cancer is well-established. *FGFR2* gene amplification and FGFR2 protein overexpression (especially of C-terminally truncated products) occurs in primary ER^+ breast cancer (Adnane et al., 1991; Katoh, 2003). The C-terminally truncated product can activate signalling cascades in a ligand-independent manner (Moffa and Ethier, 2007). Missense point mutations also occur in primary breast cancer (Stephens et al., 2005) and single nucleotide polymorphisms in intron 2 of FGFR2 are associated with an increased risk of ER^+ breast cancer (Easton et al., 2007). Our findings suggest FGFR2 and PTPRB should be considered as part of an integrated signalling pathway when assessing the activity of receptor tyrosine kinase signalling cascades in breast cancer.

Our study does have limitations, including potential off-target and non-specific toxic effects of shRNA, as well as potential variable levels of viral infection and variable tropisms to different cell types. To offset the issue of infection levels, we chose a minimum cut-off of 30% GFP-positive cells for analysis of organoids based on previously published work (Macias et al., 2011). Furthermore, the pattern of expression of FGF receptors in organoid cultures is unknown and any period of culture might alter the behaviour of epithelial cell subtypes compared with the *in vivo* situation. Nevertheless, the results of the study as a whole are consistent in supporting a role for PTPRB in regulating FGF-dependent branching morphogenesis.

We cannot definitively distinguish between a role for PTPRB in TEB bifurcation, ductal elongation or lateral branching. However, the increased density of branching shown in *Ptprb* transplant outgrowths must have resulted from either a decrease in the rate of ductal elongation or an increase in the rate of formation of new branch points (either by TEB bifurcation or lateral branching). *Ptprb* knockdown resulting in a decrease in ductal elongation would not be consistent with our *in vitro* findings that *Ptprb*-knockdown organoids have more branches in response to FGF treatment. Furthermore, higher expression of *Ptprb* in subtending ducts relative to TEBs is at least correlative evidence that *Ptprb* could be suppressing lateral branching during ductal elongation, although the TEBs versus ducts study was carried out using C57/Bl6 mice, rather than FVB/N, and the possibility of strain-specific differences cannot be definitively excluded. Despite this caveat, when considered as a whole the data favour a model in which PTPRB is a negative regulator of FGFR-dependent branching, rather than ductal elongation.

PTPRB has been typically characterised as a 'vascular endothelial-specific' phosphatase (Behjati et al., 2014). However, it is becoming clear that it has a wider role in other tissues. Its function in branching morphogenesis in both the vasculature and, as we have now shown, the mammary epithelium suggests that PTPRB is a fundamental regulator of this developmental programme irrespective of organ system. Furthermore, its emerging role in cancer and the established importance of the pathway it regulates to tumour biology, reaffirm the relevance of developmental signalling programmes to the biology of malignant disease.

MATERIALS AND METHODS

Preparation of mammary epithelial cells for flow cytometry

All animal work was carried out under UK Home Office project and personal licences following local ethical approval by the Institute of Cancer Research Animal Ethics Committee and in accordance with local and national guidelines. Single cells were prepared from fourth mammary fat pads of virgin female FVB/N mice as described (Regan et al., 2013) and stained with anti-CD24-FITC (clone M/69 at 1.0 µg/ml; BD Biosciences, 553261), anti-Sca-1-APC (clone D7 at 1.0 µg/ml; eBioscience, 17-5981), anti-CD45-PE-Cy7 (clone 30-F11 at 1.0 µg/ml; BD Biosciences, 552848), anti-CD49f-PE-Cy5 (clone GoH3 at 5.0 µl/ml; BD Biosciences, 551129) and anti-c-Kit-PE (clone 2B8 at 1.0 µg/ml; BD Biosciences, 553355). Mammary epithelial cell subpopulations were defined as shown in Fig. S1. For sorting of GFP^+ cells harvested from transplanted fat pads, the combination of anti-CD24-Pacific Blue (clone M/69 at 1.0 µg/ml; BD Biosciences, 561079), anti-Sca-1-APC, anti-CD45-PE-Cy7 and DAPI was used. DAPI-positive dead cells are distinguishable from Pacific Blue-stained cells by their very bright fluorescence.

Gene expression analysis by quantitative real-time RT-PCR (qPCR)

Freshly sorted primary cells were lysed in RLT buffer (Qiagen) and stored at −80°C. Total RNA was extracted using an RNeasy MinElute Kit (Qiagen), according to the manufacturer's instructions. For cultured organoids, RNA was isolated with Trizol (Invitrogen). qPCR reactions were performed as previously described using either TaqMan assays or in-house designed probes (Table S2) (Kendrick et al., 2008). All results were calculated using the ΔΔCt method compared with an endogenous control gene. Data were expressed as the mean fold gene expression difference in three independently isolated cell preparations over a comparator sample with 95% confidence intervals.

RNAScope *in situ* hybridisation for *Ptprb*

RNAScope for *Ptprb* was performed on 5 µm sections using RNAscope 2.5 HD Duplex Reagent Kit using manufacturer's instructions (Advanced Cell Diagnostics). RNAscope Control Slides -Mouse 3T3 Cell Pellet were used to test the protocol. Briefly, sections were cut and left to dry overnight at room temperature. Samples were then baked at 60°C for 1 h, then de-paraffinisation was performed (2×5 min in fresh xylene), which was followed by 2×1 min in 100% ethanol. Sections were then left to dry for 5 min at room temperature. Pretreat1 (H_2O_2) was then applied and left 10 min at room temperature followed by two washes in distilled H_2O. Slides were then left to boil in Pretreat2 (antigen retrieval) for 15 min and were then washed twice in distilled water (2×5 min). Preatreat3 (protease) was applied on the slides for 30 min at 40°C. After two brief washes in distilled water, warmed probes were applied for 2 h at 40°C: RNAscope 2-plex Negative Control Probe (320751), Mm-Ptprb Cat No. 481391 in C2 channel (red), RNAscope 2.5 Duplex Positive Control Probe (Mm) PPIB-C1 (Green)/ POLR2A-C2 (Red). After two washes in the wash buffer, slides were left at room temperature overnight in 5×SSC. The next day, slides were incubated with several rounds of amplification Amp1-10 reagents following manufacturer's instruction to detect red and green signal. Slides were finally counterstained for 5 s in 50% filtered Mayer's Haemalum (Lamb/ 170D) and washed briefly in water then baked for 30 min at 60°C. The slides were mounted using Vectamount (60 ml) (Vector Laboratories, 321584).

Development (2017) 144, 3777-3788 doi:10.1242/dev.149120

Isolation of TEB and duct fragments

Stromal-free TEBs and ducts were isolated as described previously (Morris and Stein, 2017; Morris et al., 2006). Briefly, C57BL/6 mice were humanely killed at 6-7 weeks (16-18 g) and the inguinal mammary glands were dissected and collected in chilled L15 medium. Twenty glands were pooled for each preparation, coarsely cut with scalpels and digested with 1 mg/ml (w/v) collagenase Type II (Sigma) at 37°C for 20-30 min (for TEBs) or 30-45 min (for ducts) with mild agitation. After incubation, the epithelium was further freed of the stroma by vigorous shaking by hand. The collagenase was diluted and blocked with fresh cold L15 medium with 0.1% fetal bovine serum (FBS) and the epithelium spun down at 250 ***g*** for 5 min. The pellet was re-suspended in fresh cold L15 medium with 10% FBS, transferred to a gridded 60 mm dish, and released TEB and ducts were collected under a stereo dissection microscope with a 10 µl pipette into 50-100 µl TRI-reagent (Sigma) before snap-freezing.

RNA isolation and microarray hybridisation from isolated epithelium

For RNA isolation, frozen samples were thawed and RNA isolated according to manufacturer's protocol before re-suspension in RNase-free water. The RNA was quantified with a Nanodrop ND-1000 spectrophotometer, pooled and subjected to on-column DNase I treatment (Qiagen) and further concentration using a RNeasy-Micro kit (Qiagen). RNA quality was finally assessed using a 2100 Bioanalyzer and RNA 6000 Nano kit (both Agilent).

For microarray hybridisation, 1.5 µg RNA per sample (from ∼300-400 isolated TEBs or ducts) was used in pooled duplicates and analysed at the Henry Wellcome Functional Genomics Facility (Glasgow). rRNA was removed using a RiboMinus Human/MouseTranscriptome Isolation kit and RiboMinus magnetic beads, labelled according to manufacturer's protocol and finally hybridised to mouse whole-genome exon arrays (GeneChip-Mouse-Exon-1.0-ST-Array, Affymetrix UK) using a GeneChip Fluidics Station 450/250. The signals were measured using a GeneChip Scanner 3000 7G. CEL-files were analysed and normalised by RMA using the open-source 'Altanalyze' software (Emig et al., 2010). Results of differentially abundant RNAs in TEBs and ducts were ranked according to raw *P*-value [one-way analysis of variance (ANOVA)] (Table S1). Raw data files have been submitted to Gene Expression Omnibus with the accession number GSE94371.

Lentivirus production

Oligonucleotide pairs for shPtprb#1 (CACCGCGTCACCCTGTAACTT-TAGCCGAAGCTAAAGTTACAGGGTGACGC and AAAAGCGTCA-CCCTGTAACTTTAGCTTCGGCTAAAGTTACAGGGTGACGC) and shPtprb#2 (CACCGCAAACACCTCCTTGGCTATCCGAAGATAGCCA-AGGAGGTGTTTGC and AAAAGCAAACACCTCCTTGGCTATCTTC-GGATAGCCAAGGAGGTGTTTGC) were ligated into pENTR/U6 Gateway system entry vector (Invitrogen) according to the manufacturer's instructions. Hairpin sequences were verified and then transferred, together with the U6 promoter, into a Gateway-modified pSEW lentiviral vector backbone (Vafaizadeh et al., 2010) by LR reaction (Invitrogen). Viral supernatants were generated by Lipofectamine 2000 (Invitrogen, 11668-019) co-transfection of the packaging and viral DNA sequence plasmids into HEK293T cells. Cells were re-fed with fresh medium (Dulbecco's Modified Eagle's Medium, DMEM; Invitrogen) plus 10% fetal calf serum (FCS) (PAA Laboratories, GE Healthcare) after 24 h. Supernatants were harvested 48 and 72 h after transfection and assayed for absence of replication-competent virus. Supernatants were stored at −80°C until use. For transplantation assays, primary mammary cells were transduced with lentivirus using the suspension method as described (Kendrick et al., 2008). Supernatants were adjusted by dilution where necessary to ensure comparable viral titres prior to transduction.

Mammary epithelial cell transplantation

Transplantation of lentivirus-transduced primary FVB/N mouse mammary epithelial cells into cleared fat pads of athymic Ncr Nude mice was carried out as described (Britt et al., 2009; Sleeman et al., 2007). Fat pads were harvested 8 weeks after transplantation, whole-mounted and photographed under epifluorescent illumination. For size analysis, the area of the GFP^+ outgrowths (defined by a continuous line around the outermost limit of the outgrowth) was determined using ImageJ with reference to a scale bar. For branching analysis, the number of branch points was counted in three 0.1 cm^2 fields per view per gland. The small size and difficulty in obtaining clear images of some outgrowths meant that not all of the outgrowths analysed for size were available for branching analysis.

Mice were injected with control and knockdown cells in contralateral fat pads (shLuc versus shPtprb pool; shScr1 versus shPtprb 0145; shScr1 versus shPtprb 3820) to control for variability in growth between animals and variability in time at which glands were harvested, both of which will affect the size of the final outgrowth.

For flow-sorting analysis, GFP^+ outgrowths were dissected out and processed to single cells, stained and analysed as described above. For secondary transplantation, GFP^+ outgrowths were dissected out, processed to single cells and immediately re-transplanted. For histological analysis of transplants, small (5 mm^3) pieces of GFP^+ outgrowths were dissected out, formalin-fixed and paraffin embedded by standard methods. Dewaxed and re-hydrated sections underwent antigen retrieval in citrate buffer (0.01 M, pH 6.0) for 18 min in a microwave (900 W) before blocking in DAKO REAL Peroxidase blocking solution for 10 min (Dako) for 30 min. Sections were incubated in Mouse on Mouse (M.O.M.) Mouse Ig blocking reagent (Vector Laboratories, BMK-2202) for 60 min followed by primary antibody for 60 min at room temperature, followed by M.O.M. Biotinylated Anti-mouse IgG Reagent for 10 min. The secondary antibody was detected by application of Vectastain Elite ABC reagent for 5 min followed by application of the chromogen 3,3'-diaminobenzidine (DAB) for 5 min (ABC, Vector Laboratories). Primary antibodies used were anti-K8/18 (clone Ks18.04, mouse monoclonal; Progen Biotechnik, 61028; 1:2), anti-SMA (clone 1A4, mouse monoclonal; Sigma, A5691; 1:500).

For immunofluorescence, sections were incubated in Mouse on Mouse (M.O.M.) Mouse Ig blocking reagent for 60 min, followed by overnight incubation in primary antibody at 4°C. Primary antibody was detected with an appropriate Alexa Fluor-conjugated secondary antibody. Images of stained sections were captured using a Leica TCS-SP2 microscope in three or four channels using Leica LCS software (Leica Microsystems). Negative controls were performed using the same protocols with substitution of the primary antibody with IgG matched controls. In double-staining experiments, control single-stained sections in which either the primary antibody was left out or the primary antibody was combined with the wrong secondary antibody showed no staining. Primary antibodies used were anti-SMA (clone 1A4, mouse monoclonal; Sigma, A5691; 1:500), anti-Ki67 (rabbit polyclonal; Abcam, ab16667; 1:300), anti-cleaved caspase-3 (rabbit polyclonal; Cell Signaling Technology, 9661S; 1:100). Lung tissue from mice treated with four doses of doxorubicin at 2.5 mg kg^{-1} and cyclophosphamide at 40 mg kg^{-1} at 5-day intervals and then harvested 5 days after the final dose was used a positive control for cleaved caspase-3.

Isolation and culture of mammary gland organoids

Cultures were prepared as previously described (Ewald et al., 2008; Fata et al., 2007). Briefly, third and fourth mammary fat pad pairs were harvested from virgin female 8- to 10-week-old FVB/N mice. Fat pads were minced and tissue shaken for 30-45 min at 37°C in 50 ml 1:1 DMEM:Ham's F12 (Invitrogen), 5% FCS (PAA Laboratories) media with 3 mg/ml collagenase A (Roche Life Sciences) and 3 mg/ml trypsin (Sigma). The collagenase solution was centrifuged at 1500 rpm (430 ***g***) for 10 min, dispersed through 10 ml 1:1 DMEM:Ham's F12, centrifuged at 1500 rpm for 10 min, and then re-suspended in 5 ml 1 µg/ml DNase I (Sigma) in serum-free 1:1 DMEM: Ham's F12 medium. The DNase solution was shaken by hand at room temperature for 2-5 min then centrifuged at 1500 rpm for 10 min. Organoids were separated from single cells through four differential centrifugations (pulse to 1500 rpm in 10 ml 1:1 DMEM:Ham's F12). The final pellet was re-suspended in the desired amount of Growth Factor Reduced Matrigel (BD Biosciences) or 1:1 mix of Growth Factor Reduced Matrigel and lentivirus or 1:1 DMEM:Ham's F12 for non-infected controls.

Organoid assays were carried out in 24-well plates. Fifty microlitres of cold Growth Factor Reduced Matrigel was laid onto a sterile 13 mm diameter borosilicate glass coverslip and incubated for 30 min at 37°C to solidify. Fifty microlitres of the organoid and Matrigel mix or organoid, Matrigel and lentivirus mix was plated over the solidified Matrigel and the plate incubated

Development (2017) 144, 3777-3788 doi:10.1242/dev.149120

at 37°C for another 30 min. Once the Matrigel or 1:1 Matrigel:lentivirus mix containing the organoids had set, the organoids were covered with minimal media (1:1 DMEM:Ham's F12, 5 µg/ml insulin; Sigma) or branching medium (minimal medium+50 ng ml^{-1} FGF2; Peprotech). ANG1 and ANG2 were a kind gift of Dr Andy Reynolds (Institute of Cancer Research, London, UK) and were also added at 50 ng ml^{-1}. For lentiviral transduction experiments, organoids with a minimum of ≥30% GFP-positive cells were analysed, in line with previous studies (Macias et al., 2011).

Protein analysis

Transduced mammary organoids were serum starved for 12 h and left unstimulated or stimulated with 10 ng/ml FGF2 for the indicated times. ERK1/2 inhibitor SCH772984 was obtained from Selleckchem (Newmarket, Suffolk, UK; S7101). Organoids were released from Matrigel using non-enzymatic cell recovery solution (BD Biosciences) and then lysed in Laemmli buffer (2% SDS, 10% glycerol, 1.25% β-mercaptoethanol, 0.002% Bromophenol Blue, 0.0625 M Tris pH 6.8). Following SDS-PAGE, protein extracts were transferred to a PVDF membrane and probed with antibodies to p44/42 MAPK (ERK1/2) (Cell Signaling Technology, 9102), phospho-p44/42 MAPK (ERK1/2) (Thr202/Tyr204) (Cell Signaling Technology, 9101), phospho-FGF receptor (Tyr653/654) (Cell Signaling Technology, 3471), FGFR1 (rabbit monoclonal, clone D8E4; Cell Signaling Technology, 9740), FGFR2 (mouse monoclonal, clone 1G3; Abnova, H00002263-M01), FGFR3 (rabbit polyclonal; Thermo Fisher Scientific, PA5-34574), FGFR4 (rabbit polyclonal; Sigma-Aldrich, HPA028251) or anti-tubulin (clone BM1A; Sigma, T6199). After incubation with peroxidase-conjugated secondary antibodies, immunocomplexes were detected using Enhanced Chemiluminescent (ECL) reagents (Millipore, Thermo Fisher). Densitometric analysis was performed using ImageJ software.

Statistics

Significance of gene expression differences analysed by qPCR were determined using 95% confidence intervals as described (Cumming et al., 2007). To test whether *Ptprb* knockdown decreased size of outgrowths but increased branching, one-tailed unpaired *t*-tests were used. To determine whether *Ptprb* knockdown increased levels of ERK1/2 and FGFR phosphorylation in response to FGF2 stimulation, one-tailed unpaired *t*-tests were used. To determine differences in organoid branching, χ^2 test of distribution of categorical variables was used.

Acknowledgements

The authors would like to thank Fredrik Wallberg, David Robertson and the Breast Cancer Now Histopathology Core Facility for technical assistance.

Competing interests

The authors declare no competing or financial interests.

Author contributions

Conceptualization: M.J.S.; Methodology: K.J.S., B.A.G.; Formal analysis: K.J.S., G.T., H.K., V.M., D.O.-D., J.S.M., T.S., C.M.I., M.J.S.; Investigation: K.J.S., G.T., H.K., V.M., D.O.-D., J.S.M., T.S.; Writing - original draft: K.J.S., C.M.I., M.J.S.; Writing - review & editing: K.J.S., G.T., H.K., V.M., D.O.-D., J.S.M., T.S., B.A.G., C.M.I., M.J.S.; Supervision: B.A.G., C.M.I., M.J.S.; Project administration: M.J.S.; Funding acquisition: M.J.S.

Funding

This study was funded by an Institute of Cancer Research PhD studentship, Wales Cancer Research Centre (G.T.), Breast Cancer Now (CTR-Q4-Y1 to C.M.I.), Cancer Research UK (A15938 to M.J.S.) and Cardiff University (M.J.S.). We acknowledge NHS funding to the National Institute for Health Research Royal Marsden Biomedical Research Centre.

Data availability

Raw data files for microarray studies have been submitted to Gene Expression Omnibus with accession number GSE94371.

Supplementary information

Supplementary information available online at
http://dev.biologists.org/lookup/doi/10.1242/dev.149120.supplemental

References

Adnane, J., Gaudray, P., Dionne, C. A., Crumley, G., Jaye, M., Schlessinger, J., Jeanteur, P., Birnbaum, D. and Theillet, C. (1991). BEK and FLG, two receptors to members of the FGF family, are amplified in subsets of human breast cancers. *Oncogene* **6**, 659-663.

Andrechek, E. R., White, D. and Muller, W. J. (2005). Targeted disruption of ErbB2/Neu in the mammary epithelium results in impaired ductal outgrowth. *Oncogene* **24**, 932-937.

Backes, C., Harz, C., Fischer, U., Schmitt, J., Ludwig, N., Petersen, B. S., Mueller, S. C., Kim, Y. J., Wolf, N. M., Katus, H. A. et al. (2014). New insights into the genetics of glioblastoma multiforme by familial exome sequencing. *Oncotarget* **6**, 5918-5931.

Ball, S. M. (1998). The development of the terminal end bud in the prepubertal-pubertal mouse mammary gland. *Anat. Rec.* **250**, 459-464.

Barr, A. J., Ugochukwu, E., Lee, W. H., King, O. N. F., Filippakopoulos, P., Alfano, I., Savitsky, P., Burgess-Brown, N. A., Müeller, S. and Knapp, S. (2009). Large-scale structural analysis of the classical human protein tyrosine phosphatome. *Cell* **136**, 352-363.

Baumer, S., Keller, L., Holtmann, A., Funke, R., August, B., Gamp, A., Wolburg, H., Wolburg-Buchholz, K., Deutsch, U. and Vestweber, D. (2006). Vascular endothelial cell-specific phosphotyrosine phosphatase (VE-PTP) activity is required for blood vessel development. *Blood* **107**, 4754-4762.

Behjati, S., Tarpey, P. S., Sheldon, H., Martincorena, I., Van Loo, P., Gundem, G., Wedge, D. C., Ramakrishna, M., Cooke, S. L., Pillay, N. et al. (2014). Recurrent PTPRB and PLCG1 mutations in angiosarcoma. *Nat. Genet.* **46**, 376-379.

Britt, K. L., Kendrick, H., Regan, J. L., Molyneux, G., Magnay, F. A. Ashworth, A. and Smalley, M. J. (2009). Pregnancy in the mature adult mouse does not alter the proportion of mammary epithelial stem/progenitor cells. *Breast Cancer Res.* **11**, R20.

Chodosh, L. A., Gardner, H. P., Rajan, J. V., Stairs, D. B., Marquis, S. T. and Leder, P. A. (2000). Protein kinase expression during murine mammary development. *Dev. Biol.* **219**, 259-276.

Cumming, G., Fidler, F. and Vaux, D. L. (2007). Error bars in experimental biology. *J. Cell Biol.* **177**, 7-11.

Ding, L., Kim, M., Kanchi, K. L., Dees, N. D., Lu, C., Griffith, M., Fenstermacher, D., Sung, H., Miller, C. A., Goetz, B. et al. (2014). Clonal architectures and driver mutations in metastatic melanomas. *PLoS ONE* **9**, e111153.

Dominguez, M. G., Hughes, V. C., Pan, L., Simmons, M., Daly, C., Anderson, K., Noguera-Troise, I., Murphy, A. J., Valenzuela, D. M., Davis, S. et al. (2007). Vascular endothelial tyrosine phosphatase (VE-PTP)-null mice undergo vasculogenesis but die embryonically because of defects in angiogenesis. *Proc. Natl. Acad. Sci. USA* **104**, 3243-3248.

Easton, D. F. Pooley, K. A. Dunning, A. M. Pharoah, P. D. Thompson, D. Ballinger, D. G. Struewing, J. P. Morrison, J. Field, H. Luben, R. et al. (2007). Genome-wide association study identifies novel breast cancer susceptibility loci. *Nature* **447**, 1087-1093.

Emig, D., Salomonis, N., Baumbach, J., Lengauer, T., Conklin, B. R. and Albrecht, M. (2010). AltAnalyze and DomainGraph: analyzing and visualizing exon expression data. *Nucleic Acids Res.* **38**, W755-W762.

Ewald, A. J., Brenot, A., Duong, M., Chan, B. S. and Werb, Z. (2008). Collective epithelial migration and cell rearrangements drive mammary branching morphogenesis. *Dev. Cell* **14**, 570-581.

Fata, J. E., Mori, H., Ewald, A. J., Zhang, H., Yao, E., Werb, Z. and Bissell, M. J. (2007). The MAPK(ERK-1,2) pathway integrates distinct and antagonistic signals from TGFalpha and FGF7 in morphogenesis of mouse mammary epithelium. *Dev. Biol.* **306**, 193-207.

Gross, I., Bassit, B., Benezra, M. and Licht, J. D. (2001). Mammalian sprouty proteins inhibit cell growth and differentiation by preventing ras activation. *J. Biol. Chem.* **276**, 46460-46468.

Hennighausen, L. and Robinson, G. W. (2001). Signaling pathways in mammary gland development. *Dev. Cell* **1**, 467-475.

Hens, J. R. and Wysolmerski, J. J. (2005). Key stages of mammary gland development: molecular mechanisms involved in the formation of the embryonic mammary gland. *Breast Cancer Res.* **7**, 220-224.

Katoh, M. (2003). FGFR2 and WDR11 are neighboring oncogene and tumor suppressor gene on human chromosome 10q26. *Int. J. Oncol.* **22**, 1155-1159.

Katoh, M. (2009). FGFR2 abnormalities underlie a spectrum of bone, skin, and cancer pathologies. *J. Invest. Dermatol.* **129**, 1861-1867.

Kendrick, H., Regan, J. L., Magnay, F. A., Grigoriadis, A., Mitsopoulos, C., Zvelebil, M. and Smalley, M. J. (2008). Transcriptome analysis of mammary epithelial subpopulations identifies novel determinants of lineage commitment and cell fate. *BMC Genomics* **9**, 591.

Lu, P., Ewald, A. J., Martin, G. R. and Werb, Z. (2008). Genetic mosaic analysis reveals FGF receptor 2 function in terminal end buds during mammary gland branching morphogenesis. *Dev. Biol.* **321**, 77-87.

Macias, H. and Hinck, L. (2012). Mammary Gland Development. *Wiley Interdiscip Rev Dev Biol* **1**, 533-557.

Macias, H., Moran, A., Samara, Y., Moreno, M., Compton, J. E., Harburg, G., Strickland, P. and Hinck, L. (2011). SLIT/ROBO1 signaling suppresses

Development (2017) 144, 3777-3788 doi:10.1242/dev.149120

mammary branching morphogenesis by limiting basal cell number. *Dev. Cell* **20**, 827-840.

Maeda, N. and Noda, M. (1998). Involvement of receptor-like protein tyrosine phosphatase zeta/RPTPbeta and its ligand pleiotrophin/heparin-binding growth-associated molecule (HB-GAM) in neuronal migration. *J. Cell Biol.* **142**, 203-216.

Matozaki, T., Murata, Y., Mori, M., Kotani, T., Okazawa, H. and Ohnishi, H. (2010). Expression, localization, and biological function of the R3 subtype of receptor-type protein tyrosine phosphatases in mammals. *Cell. Signal.* **22**, 1811-1817.

Moffa, A. B. and Ethier, S. P. (2007). Differential signal transduction of alternatively spliced FGFR2 variants expressed in human mammary epithelial cells. *J. Cell. Physiol.* **210**, 720-731.

Morris, J. S. and Stein, T. (2017). Pubertal Ductal Morphogenesis: Isolation and Transcriptome Analysis of the Terminal End Bud. *Methods Mol. Biol.* **1501**, 131-148.

Morris, J. S., Stein, T., Pringle, M.-A., Davies, C. R., Weber-Hall, S., Ferrier, R. K., Bell, A. K., Heath, V. J. and Gusterson, B. A. (2006). Involvement of axonal guidance proteins and their signaling partners in the developing mouse mammary gland. *J. Cell. Physiol.* **206**, 16-24.

Nawroth, R., Poell, G., Ranft, A., Kloep, S., Samulowitz, U., Fachinger, G., Golding, M., Shima, D. T., Deutsch, U. and Vestweber, D. (2002). VE-PTP and VE-cadherin ectodomains interact to facilitate regulation of phosphorylation and cell contacts. *EMBO J.* **21**, 4885-4895.

Pond, A. C., Bin, X., Batts, T., Roarty, K., Hilsenbeck, S. and Rosen, J. M. (2013). Fibroblast growth factor receptor signaling is essential for normal mammary gland development and stem cell function. *Stem Cells* **31**, 178-189.

Regan, J. L., Kendrick, H., Magnay, F.-A., Vafaizadeh, V., Groner, B. and Smalley, M. J. (2012). c-Kit is required for growth and survival of the cells of origin of Brca1-mutation-associated breast cancer. *Oncogene* **31**, 869-883.

Regan, J. L., Sourisseau, T., Soady, K., Kendrick, H., McCarthy, A., Tang, C., Brennan, K., Linardopoulos, S., White, D. E. and Smalley, M. J. (2013). Aurora A kinase regulates mammary epithelial cell fate by determining mitotic spindle orientation in a Notch-dependent manner. *Cell Rep.* **4**, 110-123.

Rios, A. C., Fu, N. Y., Lindeman, G. J. and Visvader, J. E. (2014). In situ identification of bipotent stem cells in the mammary gland. *Nature* **506**, 322-327.

Rubin, C., Zwang, Y., Vaisman, N., Ron, D. and Yarden, Y. (2005). Phosphorylation of carboxyl-terminal tyrosines modulates the specificity of Sprouty-2 inhibition of different signaling pathways. *J. Biol. Chem.* **280**, 9735-9744.

Shackleton, M., Vaillant, F., Simpson, K. J., Stingl, J., Smyth, G. K., Asselin-Labat, M.-L., Wu, L., Lindeman, G. J. and Visvader, J. E. (2006). Generation of a functional mammary gland from a single stem cell. *Nature* **439**, 84-88.

Sleeman, K. E., Kendrick, H., Ashworth, A., Isacke, C. M. and Smalley, M. J. (2006). CD24 staining of mouse mammary gland cells defines luminal epithelial, myoepithelial/basal and non-epithelial cells. *Breast Cancer Res.* **8**, R7.

Sleeman, K. E., Kendrick, H., Robertson, D., Isacke, C. M., Ashworth, A. and Smalley, M. J. (2007). Dissociation of estrogen receptor expression and in vivo stem cell activity in the mammary gland. *J. Cell Biol.* **176**, 19-26.

Soady, K. J., Kendrick, H., Gao, Q., Tutt, A., Zvelebil, M., Ordonez, L. D., Quist, J., Tan, D. W., Isacke, C. M., Grigoriadis, A. et al. (2015). Mouse mammary stem cells express prognostic markers for triple-negative breast cancer. *Breast Cancer Res.* **17**, 31.

Srinivasan, K., Strickland, P., Valdes, A., Shin, G. C. and Hinck, L. (2003). Netrin-1/neogenin interaction stabilizes multipotent progenitor cap cells during mammary gland morphogenesis. *Dev. Cell* **4**, 371-382.

Stephens, P., Edkins, S., Davies, H., Greenman, C., Cox, C., Hunter, C., Bignell, G., Teague, J., Smith, R., Stevens, C. et al. (2005). A screen of the complete protein kinase gene family identifies diverse patterns of somatic mutations in human breast cancer. *Nat. Genet.* **37**, 590-592.

Sternlicht, M. D. (2006). Key stages in mammary gland development: the cues that regulate ductal branching morphogenesis. *Breast Cancer Res.* **8**, 201.

Sternlicht, M. D., Kouros-Mehr, H., Lu, P. and Werb, Z. (2006). Hormonal and local control of mammary branching morphogenesis. *Differentiation* **74**, 365-381.

Stingl, J., Eirew, P., Ricketson, I., Shackleton, M., Vaillant, F., Choi, D., Li, H. I. and Eaves, C. J. (2006). Purification and unique properties of mammary epithelial stem cells. *Nature* **439**, 993-997.

Vafaizadeh, V., Klemmt, P., Brendel, C., Weber, K., Doebele, C. Britt, K., Grez, M., Fehse, B., Desrivieres, S. and Groner, B. (2010). Mammary epithelial reconstitution with gene-modified stem cells assigns roles to Stat5 in luminal alveolar cell fate decisions, differentiation, involution, and mammary tumor formation. *Stem Cells* **28**, 928-938.

Van Keymeulen, A., Rocha, A. S., Ousset, M., Beck, B., Bouvencourt, G., Rock, J., Sharma, N., Dekoninck, S. and Blanpain, C. (2011). Distinct stem cells contribute to mammary gland development and maintenance. *Nature* **479**, 189-193.

Wang, D., Cai, C., Dong, X., Yu, Q. C., Zhang, X. O., Yang, L. and Zeng, Y. A. (2015). Identification of multipotent mammary stem cells by protein C receptor expression. *Nature* **517**, 81-84.

Wiesen, J. F., Young, P., Werb, Z. and Cunha, G. R. (1999). Signaling through the stromal epidermal growth factor receptor is necessary for mammary ductal development. *Development* **126**, 335-344.

Williams, J. M. and Daniel, C. W. (1983). Mammary ductal elongation: differentiation of myoepithelium and basal lamina during branching morphogenesis. *Dev. Biol.* **97**, 274-290.

Winderlich, M., Keller, L., Cagna, G., Broermann, A., Kamenyeva, O., Kiefer, F., Deutsch, U., Nottebaum, A. F. and Vestweber, D. (2009). VE-PTP controls blood vessel development by balancing Tie-2 activity. *J. Cell Biol.* **185**, 657-671.

SUPPLEMENTARY MATERIAL

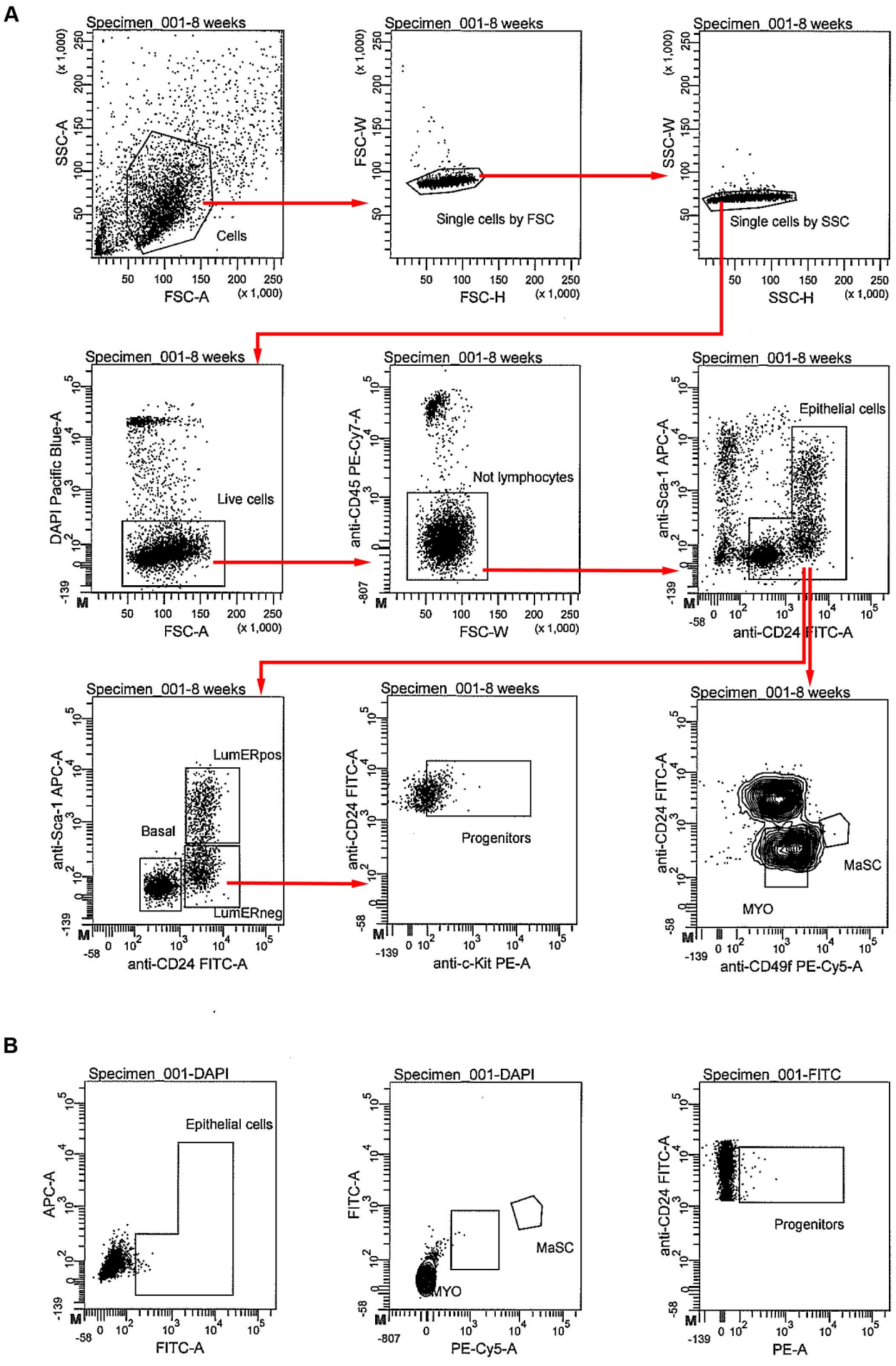

SUPPLEMENTARY FIGURE S1

Fig. S1. Flow cytometry gating workflow for isolation of mammary epithelial subpopulations. (A) Gating workflow demonstrating identification of single cells by time-of-flight analysis on forward and then side scatter, followed by exclusion of DAPI+ dead cells and CD45+ white blood cells. Remaining cells are then plotted on a Sca-1 vs CD24 plot and the epithelial cells gated as described (Britt et al., 2009). This sorting strategy isolates all mammary epithelial cells (Britt et al., 2009). The epithelial-only population is then analysed in two ways. First, it is plotted on a Sca-1 vs CD24 dot plot and the luminal ER+ and luminal ER- populations gated, with c-Kit staining of the latter being further assessed to identify the c-Kit+ progenitors. Second, the epithelial population is plotted on a CD24 vs CD49f contour plot (linear density, 5% intervals) to identify the MYOs and MaSCs, as previously described in detail (Britt et al., 2009; Soady et al., 2015). MASCs, MYOs, Luminal ER- and Luminal ER+ cells, as gated, collectively form >90% of the total mammary epithelium (Regan et al., 2012). (B) Control plots showing samples in which either only DAPI was added (left, middle) or in which the anti-c-Kit-PE was omitted (right).

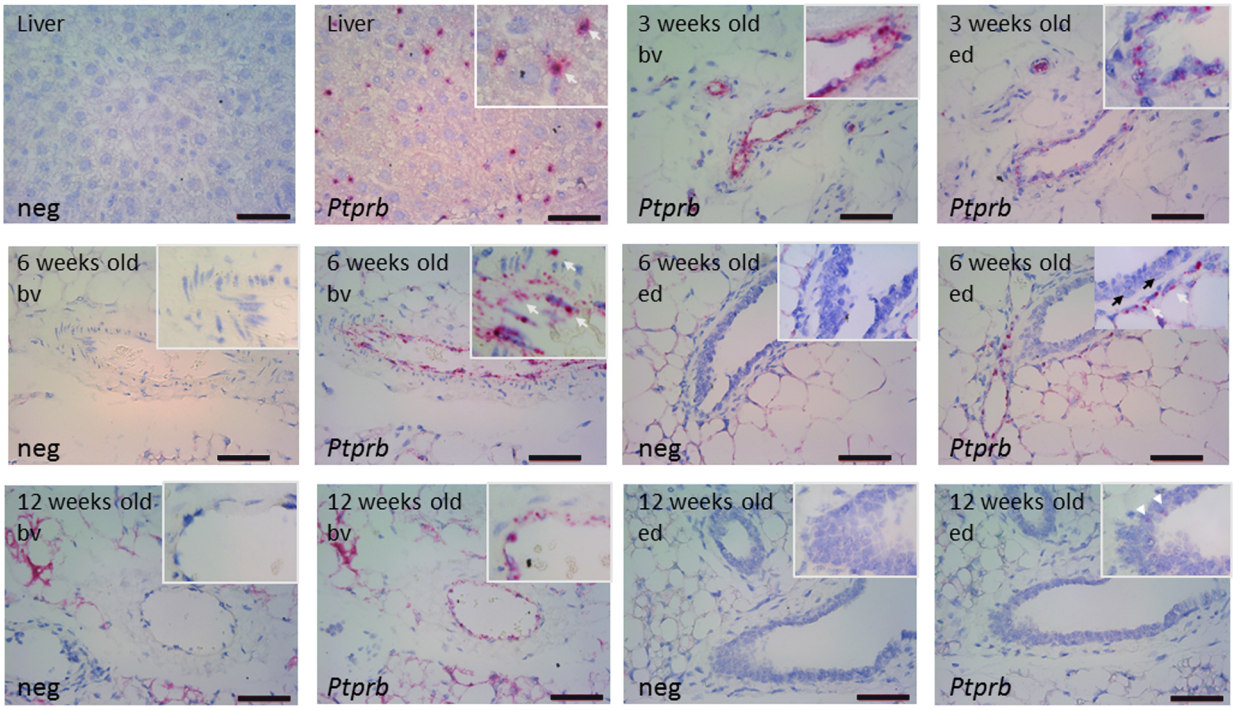

SUPPLEMENTARY FIGURE S2

Fig. S2. *Ptprb* localisation by RNAScope 2.5 HD Duplex *in situ* hybridisation. Red label indicates a positive signal. 'Neg' indicates samples labelled with the negative control probe. '*Ptprb*' indicates samples labelled with the *Ptprb* probe. 'bv' indicates a blood vessel, 'ed' epithelial duct. Bars = 50µm. Top row, liver (left two panels) used as positive control tissue, and sections from 3 week old mammary gland (right two panels). A strong, uniform *Ptprb* signal was detected on the endothelial cells lining blood vessels (middle right panel) and a positive signal was also detected in a subset of cells lining epithelial ducts (far right panel). Middle row, 6 week old mammary gland, showing a strong *Ptprb* signal on blood vessels (left two panels, white arrows on inset) and a signal on stromal cells surrounding the epithelial ducts (right panels, white arrows on inset) but no signal could be detected in the epithelium. Note that the positioning of distinctive elongated myoepithelial nuclei (black arrows on inset) demonstrate that the labelled cells are indeed outside the ducts. Bottom row, 12 week old mammary gland, again showing a strong *Ptprb* signal on blood vessels (left two panels) and a weak positive signal in a subset of cells lining epithelial ducts (right two panels, arrowheads on inset).

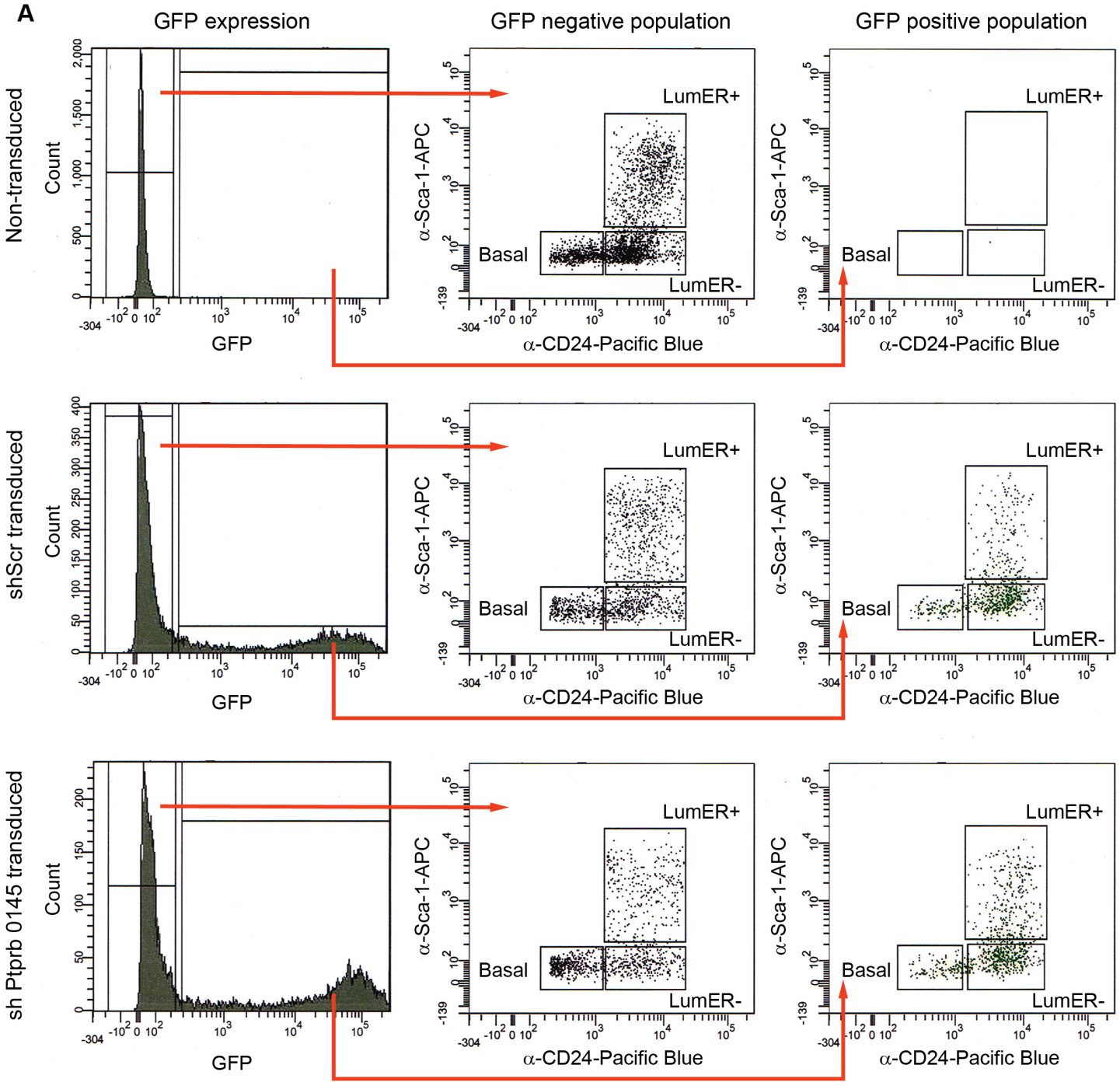

B

Percentages of epithelial subpopulations within GFP+ cells

	shScr			shPtprb 0145			shPtprb 3820		
	Mean (%)	SD (%)	n	Mean (%)	SD (%)	n	Mean (%)	SD (%)	n
Basal	11.03	3.34	6	13.73	3.35	3	16.57	10.18	3
LumERneg	55.38	5.15	6	47.87	1.99	3	47.17	4.44	3
LumERpos	28.33	4.36	6	33.30	5.84	3	29.47	6.09	3

SUPPLEMENTARY FIGURE S3

Fig. S3. *Ptprb* knockdown does not alter proportions of cell populations *in vitro*. (A) Representative flow cytometry plots form analysis of cells recovered from transplanted mammary fat pads. Only the epithelial populations are shown. Epithelial outgrowths from viral transplants consist of both transduced (GFP positive) and non-transduced cells (GFP negative) and both of these include basal, LumER- and LumER+ populations, defined by CD24 and Sca-1 expression patterns (Soady et al., 2015). Top, analysis of fat pads carrying non-transduced cells. Middle, analysis of shScr-transduced transplants. Bottom, analysis of sh Ptprb 0145-transduced transplants. **(B)** Proportions of basal, luminal ER negative and luminal ER positive cell populations in GFP+ (viral-transduced) cells harvested from fat pads transplanted with primary mammary epithelial cells transduced with shScr, shPtprb 0145 or shPtprb 3820. Data presented as mean proportion of total epithelial cells ± SD. *n* indicates number of independent transplant experiments, each of which included at least five transplanted fat pads, which contributed to the data. There are no differences between the proportions of the populations in the control compared to the knockdown transplants.

A

	Transplant Series					
	shLuc	Ptprb pool	shScr	shPtprb 0145	shScr	shPtprb 3820
Size analysis n =	8	11	9	13	14	11
Branching analysis n =	5	7	9	9	9	5

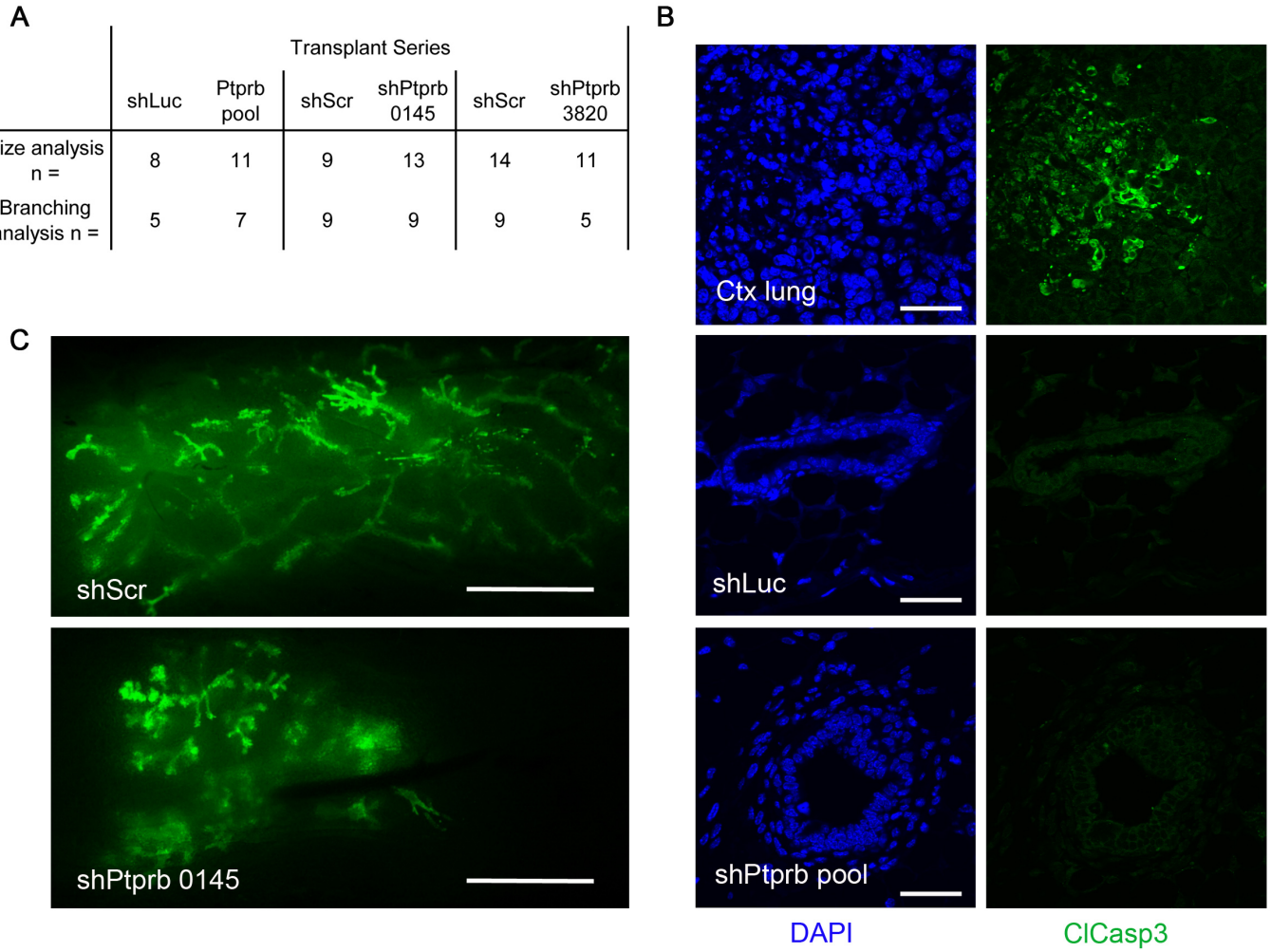

SUPPLEMENTARY FIGURE S4

Fig. S4. *Ptprb* knockdown does not enhance apoptosis. (A) Numbers of transplanted fat pads used to determine the size of outgrowths from knockdown and control cells and the amount of branching. **(B)** Cleaved Caspase-3 / DAPI staining of shLuc and shPtprb transplants, together with positive control lung tissue sample (Ctx, chemotherapy-treated). Bar = 100 μm. **(C)** Wholemounts of fat pads from secondary transplants of shScr (top) and shPtprb 0145 (bottom) transduced cells. Bars = 5 mm.

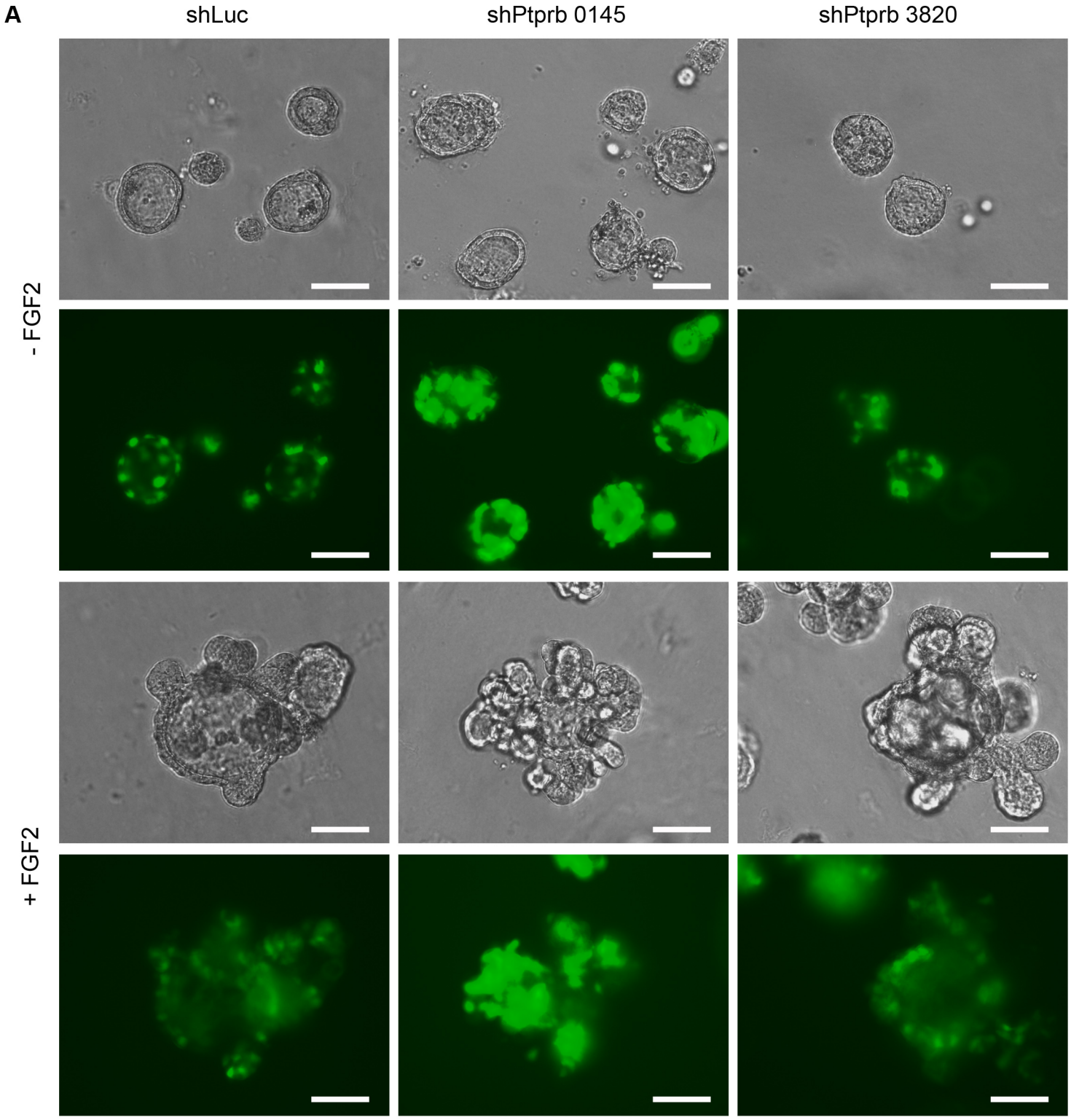

SUPPLEMENTARY FIGURE S5

Fig. S5. *In vitro* organoid branching is dependent on FGF2. (A) Transduction with shLuc, shPtprb 0145 or shPtprb 3820 in the absence of FGF2 stimulation does not cause branching. High levels of sh lentiviral transduction are indicated by strong GFP expression. Images are representative of multiple independent wells from three indpendent experiments. Paired phase contrast and GFP pictures are shown. Scale bars = 30 μm. **(B)** Examples of untreated organoids and organoids treated for seven days with 50 ng ml^{-1} FGF2, ANG1 or ANG2. Branching of organoids is only seen in FGF2 stimulated cultures. Images are representative of multiple independent wells from three independent experiments. Scale bars = 30 μm.

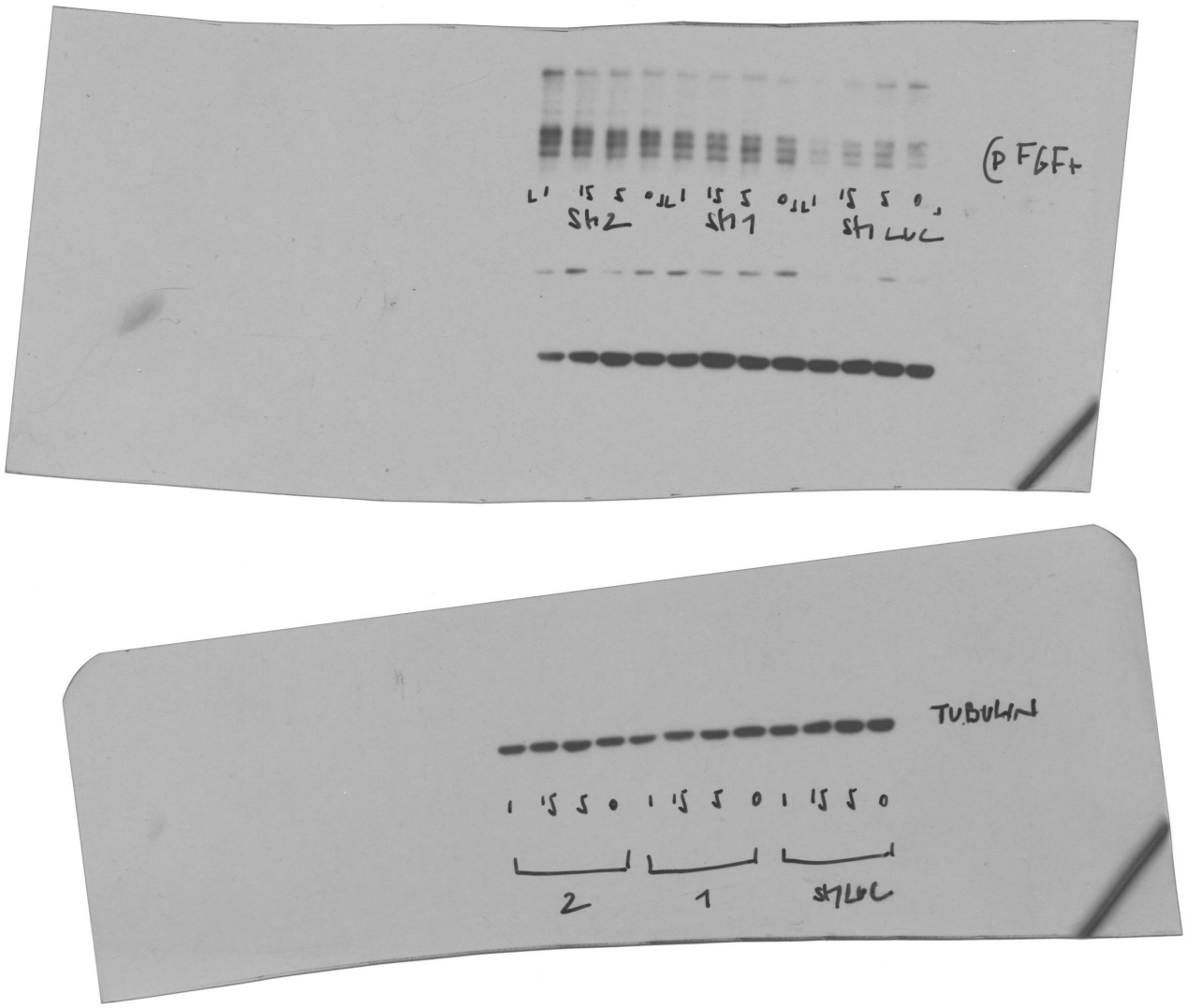

SUPPLEMENTARY FIGURE S6

Fig. S6. *Ptprb* knockdown enhances FGFR phosphorylation. Raw western blot data of effects of *Ptprb* knockdown on FGFR phosphorylation in response to FGF2 stimulation. Films of blots probed for phospho FGFR and TUBULIN are shown (blots used for preparing Figure 7A). ‘Sh1’ and ‘1’ indicate sh Ptprb 0145. ‘Sh2’ and ‘2’ indicate sh Ptprb 3820.

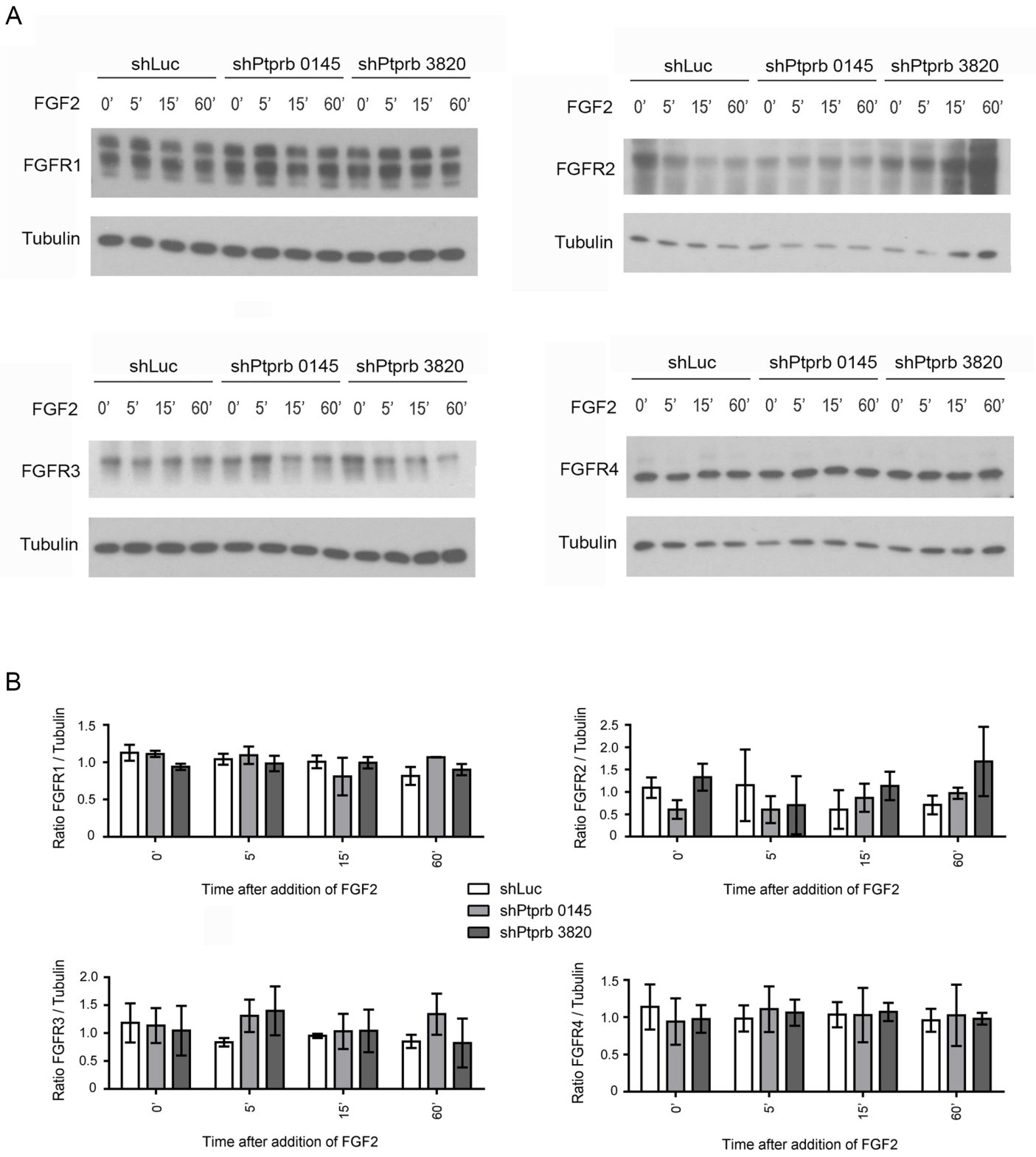

SUPPLEMENTARY DATA FIGURE S7

Fig. S7. *Ptprb* knockdown does not alter total FGFR levels. (A) Western blot analysis of total FGFR1, 2, 3 and 4 levels in organoid cultures transduced with control, 0145 or 3820 knockdown lentiviruses and either unstimulated or stimulated with FGF2. **(B)** Quantitation of total FGFR levels (mean ±SD; n=3).

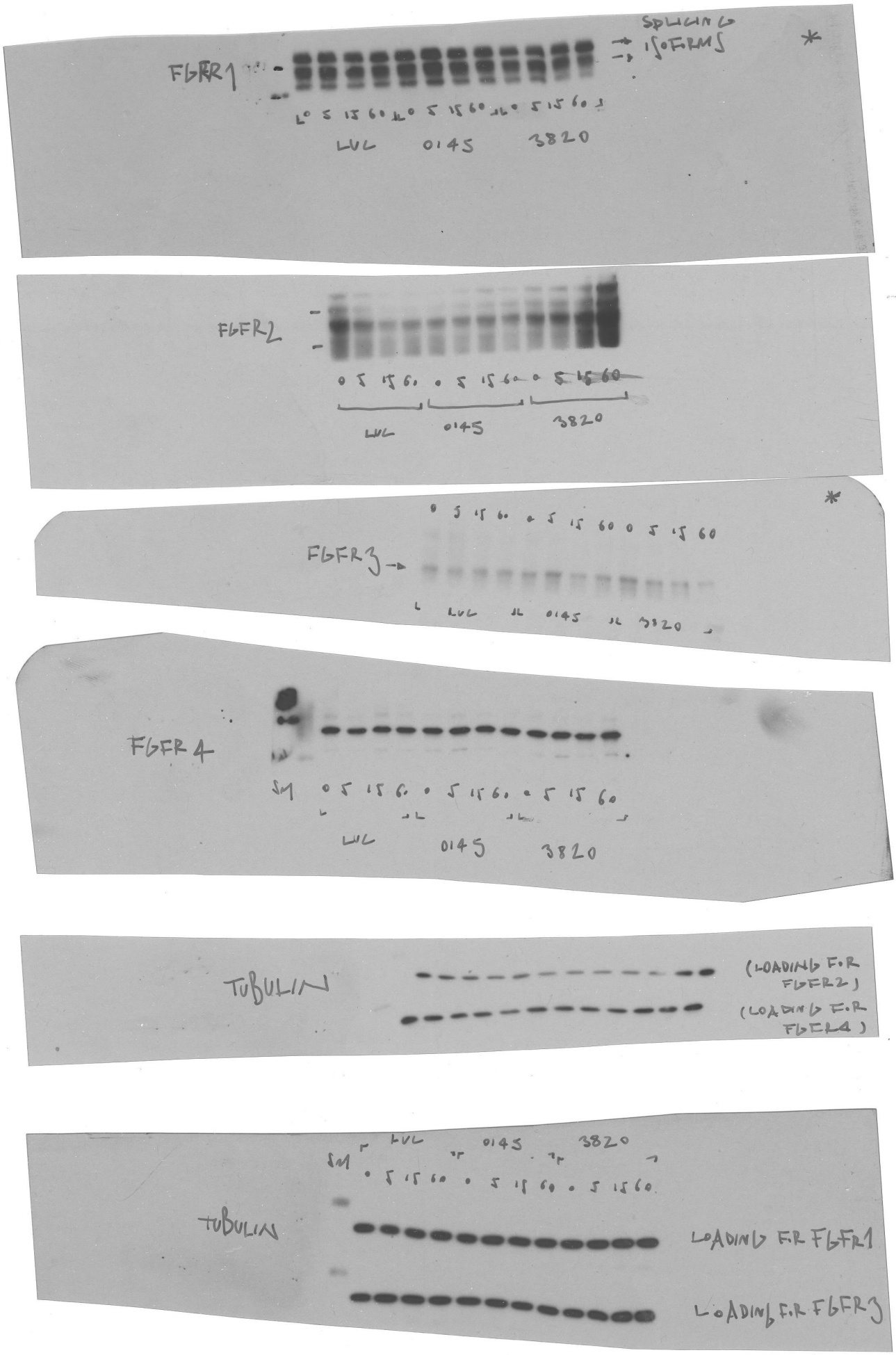

SUPPLEMENTARY FIGURE S8

Fig. S8. *Ptprb* knockdown does not alter total FGFR levels. Raw western blot data of total FGFR1, 2, 3 and 4 levels in organoid cultures transduced with control, 0145 or 3820 knockdown lentiviruses and either unstimulated or stimulated with FGF2 (blots used for preparing Supplementary Figure S7).

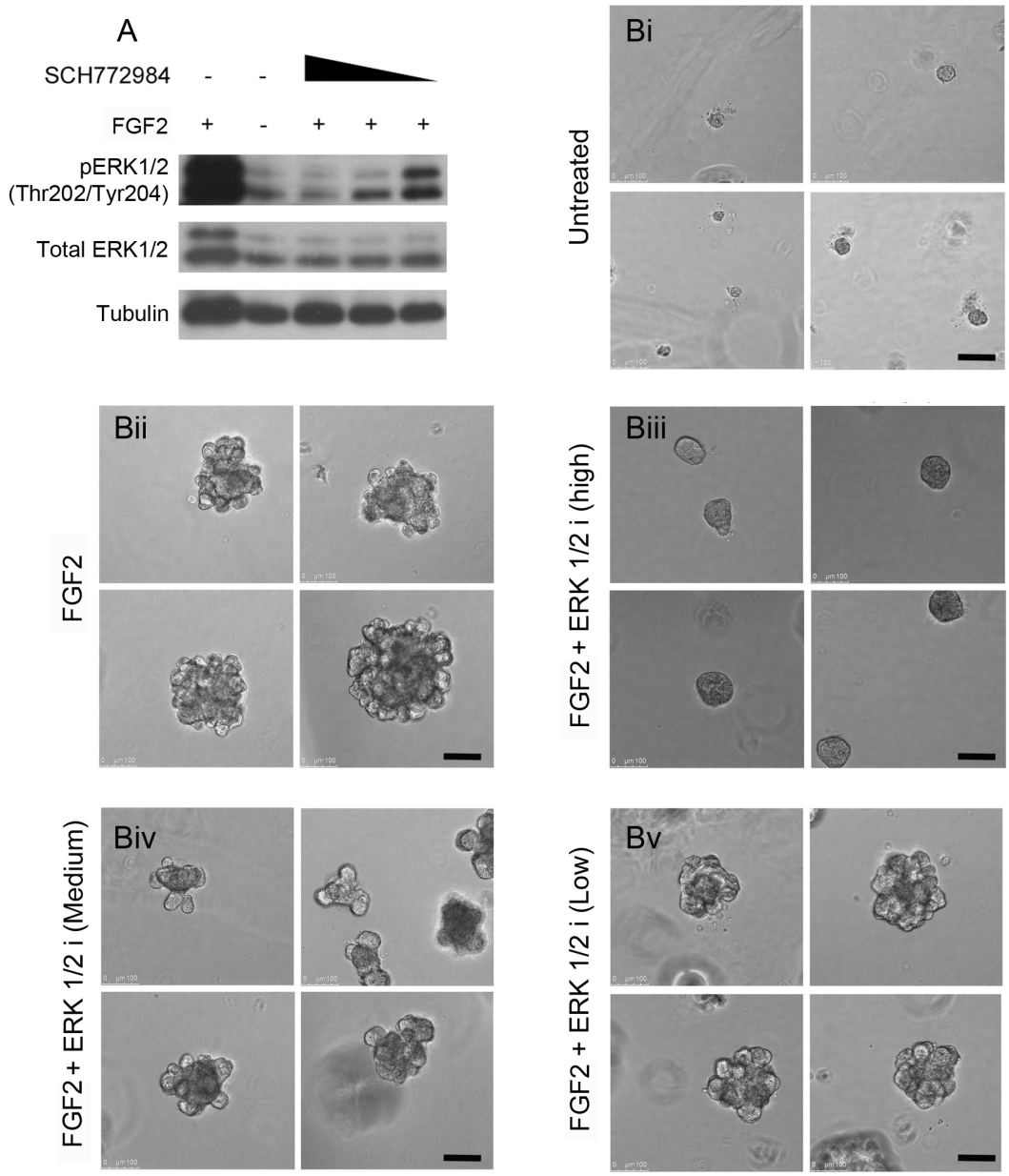

SUPPLEMENTARY FIGURE S9

Fig. S9. ERK1/2 inhibition blocks bFGF-induced mammary branching. (A) Western blot analysis of phospho- and total ERK1/2 levels in organoid cultures either unstimulated or stimulated with FGF2 and treated with High (8 nM), Medium (4 nM) or Low (2 nM) concentration of SCH772984. Tubulin was used as loading control. **(Bi - Bv)** Representative images of organoids at day 8 of culture.

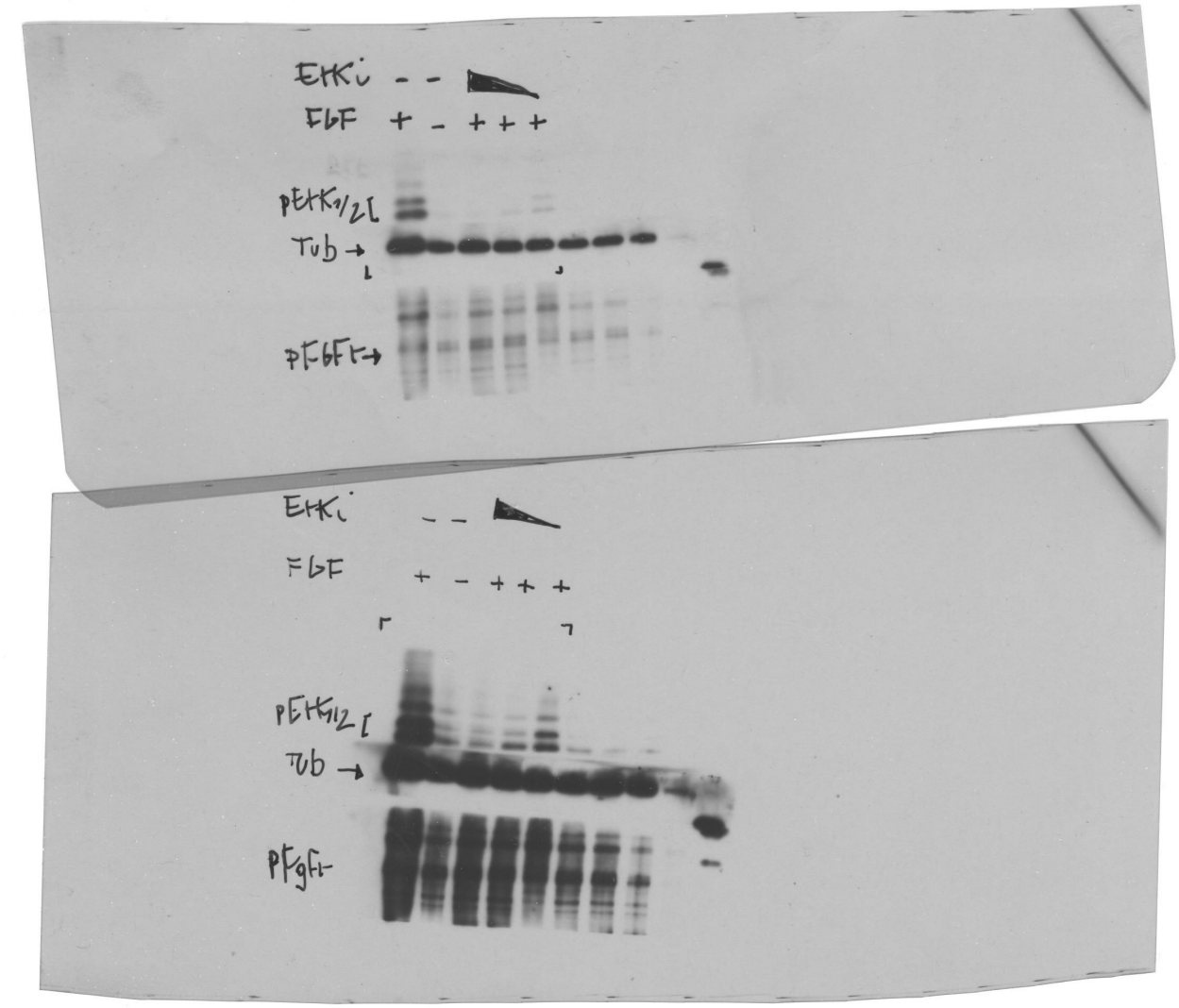

SUPPLEMENTARY FIGURE S10

Fig. S10. ERK1/2 inhibition blocks bFGF-induced mammary branching. Raw western blot data of effects of SCH772984 treatment on phospho- and total ERK1/2 in response to FGF2 stimulation. Blots probed for pERK1/2, tubulin and pFGFR (top blot, short exposure; middle blot, long exposure) and for total ERK1/2 (bottom blot). Blots used for preparing Supplementary Figure S9.

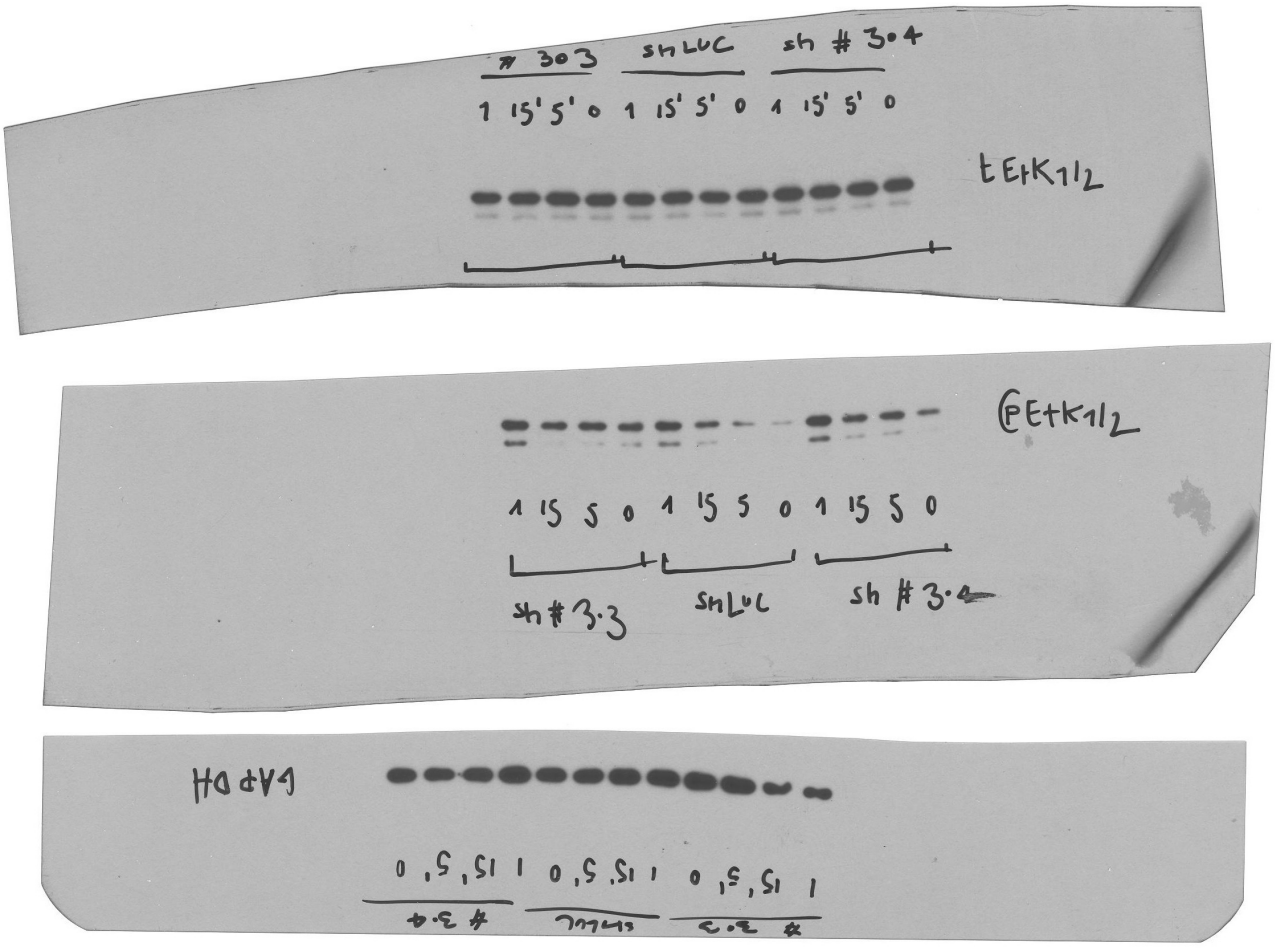

SUPPLEMENTARY FIGURE S11

Fig. S11. *Ptprb* knockdown enhances ERK1/2 phosphorylation. Raw western blot data of effects of *Ptprb* knockdown on ERK1/2 phosphorylation in response to FGF2 stimulation. Films of representative blots probed for total ERK1/2, phospho ERK1/2 and GAPDH are shown (blots used for preparing Figure 7B).

SUPPLEMENTARY TABLES

Table S1. Gene expression analysis comparing isolated TEBs vs ductal fragments. Data for 3756 genes with >1.5 fold differential expression between the two structures from two independent replicates each of which analysed TEBs and duct fragments from >100 animals.

Click here to Download Table S1

Table S2. Sybr green probes and TAQMan assays for quantitative real-time rtrPCR.

Gene	Unigene	TAQMan Assay
Actb	Mm.391967	Mm00607939_s1
Egfr	Mm. 8534	Mm00433023_m1
Erbb2	Mm. 290822	Mm00658541_m1
Fgfr1	Mm. 265716	Mm00438930_m1
Fgfr2	Mm. 16340	Mm00438941_m1
Igf1r	Mm. 275742	Mm00802831_m1

Gene	Unigene	Sybr Green probes
Actb	Mm.391967	Fwd: agcgcaagtactctgtgtgga
		Rev: gggccggactcatcgtact
Ptprb	Mm.37213	Fwd: acatttatggggcagtgcat
		Rev: gttccgcagtttctttgctc
Tek/Tie2	Mm.14313	Fwd: gacagtgctggagggagaag
		Rev: tccgcagagcagtcaattc

SUPPLEMENTARY REFERENCES

Britt, K. L., Kendrick, H., Regan, J. L., Molyneux, G., Magnay, F. A., Ashworth, A. and Smalley, M. J. (2009). Pregnancy in the mature adult mouse does not alter the proportion of mammary epithelial stem/progenitor cells. *Breast Cancer Res* **11**, R20.

Regan, J. L., Kendrick, H., Magnay, F. A., Vafaizadeh, V., Groner, B. and Smalley, M. J. (2012). c-Kit is required for growth and survival of the cells of origin of Brca1-mutation-associated breast cancer. *Oncogene* **31**, 869-83.